International Journal of Thermofluids 27 (2025) 101180

Contents lists available at ScienceDirect

International Journal of Thermofluids

journal homepage: www.sciencedirect.com/journal/international-journal-of-thermofluids

A novel photovoltaic/thermal (PVT) system using nano-enhanced micro-encapsulated PCM slurry for steam production: A numerical study

Ahmed Azmeer [a], Yahya Sheikh [b], Hasan A. Kanjo [c,*], Hamzeh Sabouni [d]

[a] Physical Science and Engineering Department, King Abdullah University of Science and Technology, Thuwal, Saudi Arabia
[b] Department of Mechanical Engineering, American University of Sharjah, Sharjah, United Arab Emirates
[c] Department of Sustainable and Renewable Energy Engineering, University of Sharjah, Sharjah, United Arab Emirates
[d] Materials Science and Engineering Program, American University of Sharjah, Sharjah, United Arab Emirates

ARTICLE INFO

Keywords:
Photovoltaic/thermal (PVT)
Semi-passive cooling systems
Phase change material
Micro-encapsulated PCM slurry
Steam production

ABSTRACT

As industries reliant on steam-based processes strive to reduce fossil fuel consumption and carbon emissions, interest in renewable technologies, particularly photovoltaic/thermal (PVT) systems that generate both thermal and electrical energy, is increasing. However, the limited thermal performance of PVT systems remains a key barrier. Traditional working fluids, such as water, nanofluids, and phase change material (PCM) slurries, exhibit low thermal conductivity, poor temperature regulation, and inefficient heat storage. To address these issues, a novel working fluid incorporating graphene oxide (GO) nanoparticles into microencapsulated PCM (MPCM) slurry is proposed. The integration of GO nanoparticles not only enhances the dispersion stability of the MPCM slurry but also significantly increases its thermal conductivity, leading to improved heat dissipation from PV cells. A comprehensive CFD investigation is conducted using ANSYS Fluent 2021, employing an Eulerian–Eulerian multiphase model to simulate the three-phase flow. In this model, water serves as the primary phase, while GO nanoparticles and MPCM function as secondary dispersed phases. The results demonstrate that increasing the GO volume fraction from 0 to 0.005 reduces average PV cell temperatures by up to 5°C at 40°C. Additionally, the nano-enhanced MPCM slurry achieves a thermal efficiency of 88.1 % and an electrical efficiency of 10.3 %. It is also found that using MPCM slurry as the working fluid, a 15 % volume fraction of MPCM with a melting point of 40°C achieves the highest thermal efficiency of 90.1 %, outperforming water by 20.1 % and surpassing previous studies on MPCM slurry and nanofluids.

1. Introduction

The worldwide need for energy is increasing at an extraordinary pace, propelled by rapid urbanization, industrial development, and population increase [1]. The heightened demand has resulted in an ongoing dependence on traditional fossil fuels, which now constitute around 81 % of global energy use [2]. Nearly 50 % of global final energy consumption comes from heat, a significantly higher share compared to transportation (30 %) and electricity (20 %) [3]. Heat is widely used in industries, residential areas, and commercial buildings, with industrial heating alone making up about 51 % of total consumption, thereby contributing to higher greenhouse gas emissions [3].

Steam generation is a fundamental aspect of many industrial processes, playing a crucial role in sectors such as food and beverage, textiles, pharmaceuticals, and energy. Beyond process heating, steam is essential for sterilization, drying, and various specialized applications. Notably, in the energy-intensive food manufacturing sector, steam systems alone account for 57 % of their primary fuel consumption [4]. The environmental consequences of this dependence are concerning, including rising greenhouse gas emissions, climate change, and habitat destruction. To mitigate these effects, renewable energy sources have emerged as a key solution for achieving a sustainable energy future.

One promising approach is the transition to electrified steam, a sustainable alternative powered by renewable energy. This shift is particularly beneficial in the food and beverage manufacturing sector, where traditional steam generation relies heavily on fossil fuel combustion, leading to substantial greenhouse gas emissions. By contrast, electrified steam systems can be powered by renewable sources such as wind, solar, or hydroelectric energy, significantly reducing the carbon footprint of manufacturing processes [5]. Beyond its environmental

* Corresponding author at: Department of Sustainable and Renewable Energy Engineering, University of Sharjah, Sharjah, United Arab Emirates.
E-mail address: u19101303@sharjah.ac.ae (H.A. Kanjo).

https://doi.org/10.1016/j.ijft.2025.101180

Available online 18 March 2025
2666-2027/© 2025 The Author(s). Published by Elsevier Ltd. This is an open access article under the CC BY-NC-ND license (http://creativecommons.org/licenses/by-nc-nd/4.0/).

advantages, electrified steam also improves energy efficiency and enhances the overall sustainability of industrial operations. By replacing conventional steam generation with electrified systems, industries can drastically reduce emissions while ensuring a more reliable and renewable energy supply [5].

In recent years, the integration of solar energy systems for steam production has attracted substantial interest as companies move toward sustainable and low-carbon energy solutions. Solar energy has attracted considerable interest because of its availability, scalability, and adaptability in fulfilling both electrical and thermal energy requirements [6].

Photovoltaic/Thermal (PVT) systems have demonstrated enormous promises for addressing these needs by offering an efficient and ecologically friendly alternative to traditional fossil-fuel-based boilers [7]. In industrial settings, steam needs vary greatly depending on the application, with temperatures ranging from low to medium levels (50°C to 250°C) in numerous operations. The use of PVT systems for steam generation not only decreases reliance on fossil fuels but also contributes to obtaining high renewable heating fractions, harmonizing with global sustainability objectives [8]. PVT systems exemplify a novel amalgamation of solar technologies, engineered to concurrently produce energy and harness useable heat [2]. PVT systems mitigate the efficiency losses associated with freestanding photovoltaic (PV) modules, which convert sunlight into electricity but are hindered by heat buildup, by harnessing surplus thermal energy. This dual capability not only improves total energy conversion efficiency but also expands the usability of solar energy for home, commercial, and industrial uses. The capacity to create both electrical and thermal energy presents PVT systems as a transformational technology in the move toward a low-carbon energy future [9].

Despite these improvements, the performance of PVT systems is still hampered by various difficulties. A significant concern is the temperature regulation of the system. As the temperature of PV modules rises, their electrical efficiency reduces dramatically, with studies estimating a loss of 0.45 % to 0.50 % in efficiency for every 1°C rise in temperature [10]. This temperature-induced efficiency loss restricts the capacity of PVT systems to achieve optimum performance, especially in places with strong solar irradiation. Moreover, the heat created inside the system is generally underused, thereby lowering the overall efficiency of the technology [10]. The need to optimize the thermal management and efficiency of PVT systems is not just a technical problem but also a prerequisite for reaching larger sustainability objectives. Solar technologies, especially PVT systems, are a cornerstone of worldwide efforts to decarbonize energy generation and fulfill climate objectives such as those stated in the Paris Agreement [11]. As enterprises and governments attempt to decrease their carbon footprints, the need for efficient, dependable, and cost-effective solar solutions continues to grow. In particular, the incorporation of modern heat management methods into PVT systems provides a road to greatly increase their performance and extend their application across numerous industries [11].

Another key motivator for expanding PVT technology is the economic potential of these systems. By absorbing and using thermal energy, PVT systems may counterbalance the need for new heating infrastructure, delivering cost reductions in both residential and industrial settings. For instance, businesses needing medium-temperature process heat, such as food and beverage, textiles, and pharmaceuticals, may profit greatly from the use of PVT systems [2]. The combined purpose of these systems in delivering energy and heat makes them a practical and economically desirable option.

Phase Change Materials (PCMs) have emerged as a possible approach for increasing thermal control and energy storage in solar energy systems. PCMs are materials capable of storing and releasing considerable quantities of latent heat during phase changes, often between solid and liquid states. This unique trait enables PCMs to collect surplus heat during times of high thermal energy availability and release it when the system wants more heat, maintaining a continuous and efficient energy supply. In the context of PVT systems, PCMs serve a significant role in minimizing temperature swings, hence increasing both the electrical and thermal performance of the system [12]. The integration of PCMs into PVT systems is prompted by the need to solve a significant restriction of solar energy technologies: the intermittent and variable nature of solar radiation. As solar irradiance changes throughout the day, the temperatures of PV modules and thermal collectors may vary dramatically, resulting in efficiency losses and thermal inefficiencies. The use of PCMs minimizes the need for external cooling methods, such as water or air-based systems, which are generally resource-intensive and less efficient in high-temperature environments [13]. Despite their promise, traditional PCMs confront various problems when used in PVT systems. One of the key drawbacks is their comparatively poor thermal conductivity, which may impede the pace at which heat is absorbed or released during phase transitions. This bottleneck may lead to uneven temperature distribution and limit the efficiency of PCM in maintaining ideal operating conditions for the PVT system. Moreover, many classic PCMs, such as paraffin-based materials, display difficulties relating to long-term stability, leakage during melting, and environmental effects. These issues need the development of improved PCM technologies that can overcome these constraints while retaining high energy storage capacity and durability [14]. Another key difficulty is the compatibility of PCMs with the operating needs of PVT systems. The selection of a suitable PCM relies on parameters such as the operating temperature range, phase transition temperature, and thermal cycling stability [14]. For instance, PCMs with phase transition temperatures that are too low may not successfully regulate the heat created by the PV modules, while those with too high transition temperatures may not adequately absorb thermal energy. Achieving an ideal equilibrium involves careful evaluation of the material attributes and the unique application demands of the PVT system [15]. Recent breakthroughs in PCM technology have focused on enhancing the thermal conductivity of PCMs embedding with highly conductive micro-particles [16], nanoparticles [17], and metal foams [18,19].

Additionally, microencapsulation methods, which include encapsulating PCMs inside protective shells, have been developed to minimize leakage and increase the mechanical stability of the material [20]. These improvements are paving the path for the mainstream deployment of PCMs in solar energy applications [21]. The function of PCMs goes beyond temperature control in PVT systems. By offering a dependable way of storing and releasing heat, PCMs also allow the integration of solar energy into applications that demand continuous and predictable thermal energy outputs, such as industrial process heating and home water heating. Furthermore, the usage of PCMs adds to the overall sustainability of solar energy systems by minimizing energy losses and enhancing resource use. As the need for efficient and sustainable energy solutions develops, PCMs are projected to become a cornerstone of advanced thermal energy storage technologies [22].

The discovery of PCM slurry marks a further step forward in energy storage and transmission technology. PCM slurry is a fluid combination in which micro-encapsulated PCMs are spread inside a base fluid, such as water or glycol. This design combines the latent heat storage capabilities of PCMs with the convective heat transmission qualities of the fluid, resulting in a flexible and effective medium for thermal management. The fluidic structure of the slurry enables it to flow across heat exchange systems, making it very versatile for use in complicated PVT settings and industrial applications needing variable energy distribution.

The economic viability of steam generation utilizing PVT systems is another major element pushing their acceptance. Compared to conventional techniques, the incorporation of sophisticated energy storage technologies lowers the need for large-scale storage tanks or extra heating equipment, greatly cutting capital and operating costs. Furthermore, PVT systems may be built to work in hybrid configurations, where solar energy is supplemented by other renewable sources or conventional boilers, assuring continuous steam delivery while limiting carbon emissions [7].

The function of steam generation goes beyond industrial uses to renewable energy systems, where it is utilized to drive turbines and create power. In this context, the capacity of PVT systems to effectively create high-temperature steam makes them a vital aspect of next-generation renewable energy solutions. By integrating solar-driven thermal energy storage with sophisticated heat transfer technologies, these systems may allow large-scale energy production with minimal environmental impact [2]. The promise for PVT systems to improve steam generation resides not only in their efficiency but also in their flexibility to diverse sizes and applications. From small-scale industrial processes to large-scale renewable energy plants, the adaptability of PVT systems, along with improvements in thermal energy storage and heat transmission, assures their relevance in different situations. This versatility, combined with their environmental and economic advantages, makes PVT systems an important component of the worldwide move toward sustainable energy systems.

Recent studies have shown that PVT systems, which combine the electricity-generating capabilities of PV panels with the heat-collecting capability of thermal collectors, have emerged as a creative and effective method for optimizing solar energy use. Recent gains in PVT systems have been spurred by innovations in material science, cooling methods, and system integration, resulting in considerable increases in both electrical and thermal efficiency. For instance, the integration of spectrum beam filters into PVT systems has permitted a decrease in operating temperatures by up to 15 %, boosting electrical efficiencies to roughly 15.75 % and thermal efficiencies to 20.9 %, significantly exceeding typical PV systems [23]. Similarly, the use of nanofluids, such as TiO_2-water and Al_2O_3-water, has received attention for their better heat transmission capabilities. Al_2O_3-water nanofluids at ideal concentrations have been found to boost thermal efficiencies by up to 63.28 %, presenting a realistic approach to prevent panel overheating while enhancing total energy production [10,24]. Advanced cooling methods have further contributed to the growth of PVT systems, with inventions such as fin turbulators in serpentine channels enhancing thermal efficiency to 59 % and delivering electrical efficiency increases of up to 1.5 % above traditional systems. PCMs have also been introduced into PVT systems as effective temperature management mechanisms, with studies indicating their potential to lower PV panel temperatures by 10–20 %, thus raising electrical output by 5–10 % and enhancing operational stability [7,25]. Additionally, bi-fluid systems that utilize both air and nanofluids have made a breakthrough in heat dissipation, with thermal efficiencies reaching up to 63 % when employing Al_2O_3-water nanofluids at 1 % concentration. These technologies not only enhance heat transfer rates but also lower the possibility of thermal hotspots, assuring the lifespan of PV panels and continuous energy output. Furthermore, hybrid concentrator technologies, such as parabolic trough concentrators (PTCs) and linear Fresnel concentrators, have enhanced the uniformity of sunlight distribution, achieving optical efficiencies of up to 49.8 % and boosting system performance by up to 20 % compared to traditional concentrators. Recent designs have also focused on small collector topologies, which minimize system footprint while retaining high efficiency, with some models attaining up to 70 % combined efficiency in residential applications [26].

Graphene, in its integrated forms such as graphene oxide (GO), nanotubes, and nanoparticles, is gaining attention for its exceptional electrical, mechanical, and thermal properties. These unique characteristics enable graphene to significantly enhance the performance of host materials and liquids, making it a promising addition to various applications, including in PVT systems. Among the known materials, graphene exhibits the highest thermal conductivity, which has attracted considerable research aimed at improving the efficiency of cooling systems [27,28]. Graphene oxide nanoparticles, in particular, offer excellent suspension stability and are well-dispersed in water, as evidenced by studies conducted by Yudong et al. [29]. Furthermore, a recent experimental study [30] found that GO nanoparticles improved the dispersion stability of MPCM slurry more effectively than TiO_2, Al_2O_3, or MPCM alone, further showcasing graphene's potential for enhancing thermal management in PVT systems. Sodium dodecyl sulfate (SDS) was used as a surfactant to improve dispersion stability, proven effective for TiO_2, GO, Al_2O_3 nanofluids, and MPCMs [30]. Hybrid suspensions were prepared by mixing MPCM capsules, nanoparticles, and SDS with water, followed by 2 h of magnetic stirring and 30 min of ultrasound treatment for uniform dispersion.

To the best of our knowledge, this study is the first to investigate the thermal and electrical performance of a PVT system in which the working fluid consists of water combined with graphene oxide (GO) nanoparticles and microencapsulated PCM to optimize energy efficiency. This innovative approach combines electricity generation through photovoltaic cells with advanced thermal collection capabilities. The integration of GO nanoparticles not only enhances the dispersion stability of the MPCM slurry but also significantly increases its thermal conductivity, leading to improved heat dissipation from PV cells. The nano-MPCM slurry serves as a sophisticated heat transfer fluid, leveraging its high thermal conductivity and exceptional latent heat storage properties to enhance the system's performance.

By utilizing this integrated approach, the objective of this study is to develop a highly efficient PVT system capable of powering an electric boiler while simultaneously preheating inlet water, thereby reducing overall energy consumption and operational costs. The nano-MPCM slurry's unique characteristics enable more effective heat transfer and storage, which significantly improves the thermal efficiency of the PVT system. This method represents a cutting-edge solution for maximizing energy utilization in water heating applications, offering a more sustainable and technologically advanced alternative to traditional energy generation and thermal management techniques.

In addition to the novel working fluid, a key innovation in this study's system is its semi-passive operation, requiring the pump to circulate the working fluid back to the tank only a few times each day. In contrast to other PVT systems that rely on continuous pump operation for heat exchange, this system uses gravity-driven flow from an elevated tank, which effectively minimizes energy consumption.

This study provides a comprehensive analysis of the thermo-fluidic interactions within the proposed system, aiming to identify the optimal configuration of the MPCM slurry. Performance is assessed based on average PV cell temperature and overall efficiency, encompassing both thermal and electrical efficiencies. The study first conducts a systematic numerical assessment of varying MPCM volume fractions at different melting temperatures, with water as the baseline for comparison. The configuration yielding the lowest average PV cell temperature and highest overall efficiency is identified as optimal. The second phase of the study investigates the effect of adding GO nanoparticles into the optimal configuration, evaluating its impact on PVT performance through key parameters: average PV cell temperature, thermal conductivity, pressure drop, overall efficiency, and temperature contour of the working fluid.

2. Methodology

In this study, a comprehensive steady-state computational fluid dynamics (CFD) simulation is employed to explore the thermal performance of a PVT system with nano-enhanced MPCM slurry as its working fluid. Using the powerful modeling tools of ANSYS Fluent, the study analyzes key thermal and fluid flow dynamics under realistic conditions to assess the system's efficiency.

2.1. Geometrical model

Fig. 1(a) illustrates the proposed PVT system, which integrates a nano-MPCM slurry as the working fluid to power an electric boiler while preheating the inlet water. A key feature of this system is its semi-passive operation, where the pump is activated only a few times daily to return the working fluid to the elevated tank. Unlike conventional PVT systems

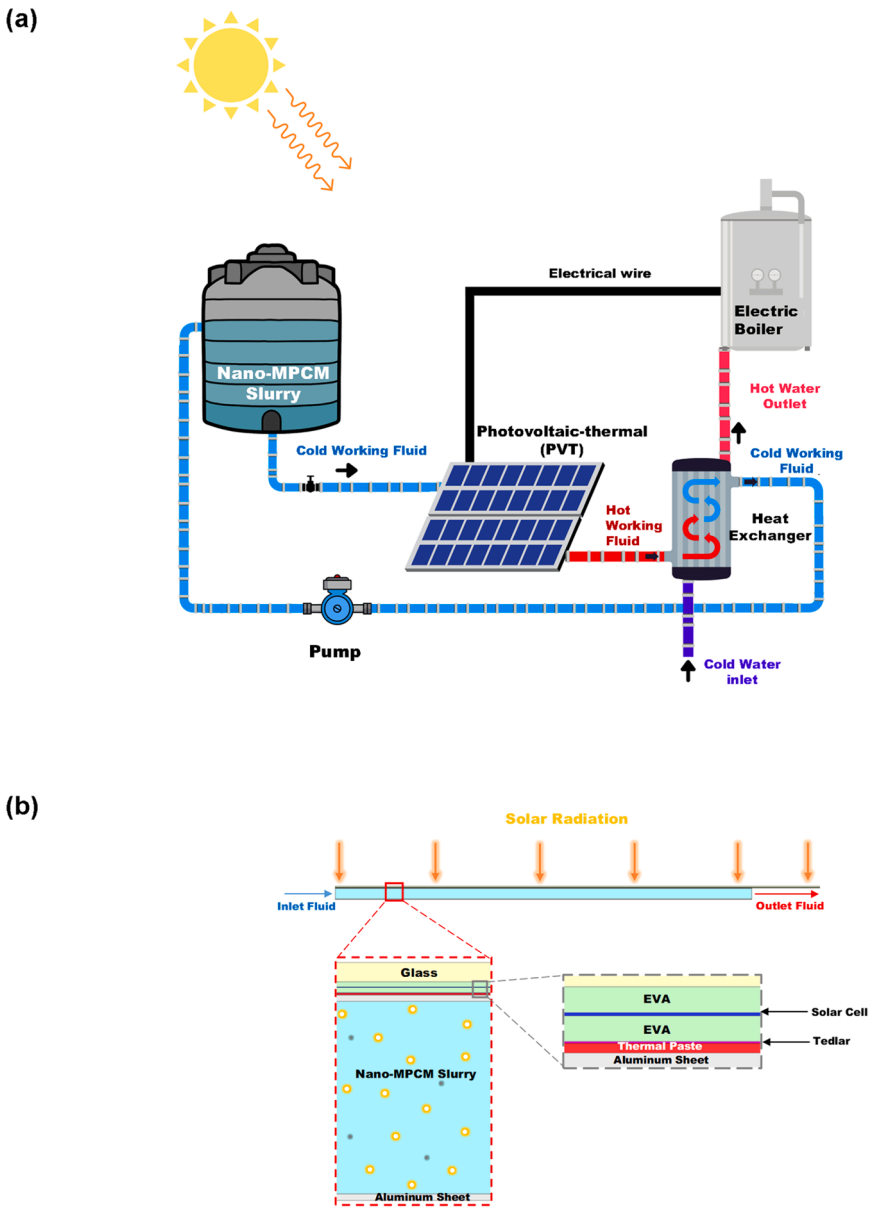


Fig. 1. A schematic representation of (a) the proposed PVT system designed to power an electric boiler while preheating the inlet water and (b) a cross-sectional view of the novel PVT system utilizing a nano-enhanced MPCM slurry.

that depend on continuous pumping for heat exchange, this system leverages the gravitational potential of the overhead reservoir tank to sustain fluid flow through the PVT collector, significantly reducing energy consumption and enhancing overall efficiency.

To assess the electrical performance of the PVT system and the thermal behavior of nano-enhanced MPCM slurry flowing through its horizontal channel, a two-dimensional model is developed using SpaceClaim software. The model comprises five solid domains for the PV module: the front cover (glass), encapsulation (ethyl vinyl acetate (EVA)), solar cells, back sheet (Tedlar), and thermal paste (serving as a

Table 1
Thickness and thermal and physical properties of each material used in the simulations [6,27,31].

Materials	Phase	Density (kg/m^3)	Thermal conductivity (W/m·K)	Heat capacity (J/kg·K)	Thickness (mm)	Latent heat (kJ/kg)
Glass	Solid	2450	2	500	3	–
EVA	Solid	950	0.311	2090	0.8	–
Solar cell	Solid	2329	148	700	0.1	–
Tedlar	Solid	1200	0.15	1250	0.05	–
Thermal paste	Solid	2600	1.9	700	0.3	–
Aluminum	Solid	2700	160	900	1	–
MEPCM particle	Liquid	1000	0.310	1754	–	167
	Solid	936	0.144	2014	–	–
Water	Liquid	997	0.610	4180	30	–
Graphene oxide	Solid	121	2100	2720	-	–

thermal conductor). The flow channel is made up of two domains: a solid domain (aluminum) and a fluid domain (a mixture of water, micro-encapsulated PCM, and GO nanoparticles), as depicted in Fig. 1(b). The thermophysical properties of the proposed PVT system are detailed in Table 1

2.2. Governing equations and boundary conditions and model assumptions

The Eulerian-Eulerian multiphase model in ANSYS Fluent 2021, solved using the Coupled Solver, is used to simulate a 2D model of PVT with a three-phase system where water is the primary (continuous) phase, and GO nanoparticles and MPCM microparticles are the secondary (dispersed) phases. This approach effectively captures the interactions between the primary fluid and the dispersed secondary phases, ensuring accurate modeling of multiphase flow dynamics. The study utilizes a pressure-based solver with the PRESTO pressure scheme, with convergence achieved in fewer than 500 iterations. In the mesh independence analysis, a 1 mm mesh size is chosen with total element numbers of 110,570, providing an optimal balance between numerical accuracy and computational efficiency.

The governing equations for our model:

The Continuity Equation of each phase [32]:

$$\nabla\cdot\left(\alpha_q\rho_q\vec{v}_q\right)=0 \tag{1}$$

The subscripts q represent the liquid phase and solid phase, α is the volume fraction of each phase (q =l, s_1,s_2) where l, s_1,s_2 represent liquid phase (water), solid phase (MPCM), and solid phase (GO nanoparticles), respectively. $\vec{v}_q$ and $\rho_q$are the velocity vector and density of each phase, respectively.

The sum of the volume fractions for all three phases must satisfy:

$$\alpha_l+\alpha_{s_1}+\alpha_{s_2}=1 \tag{2}$$

This condition ensures that the phases collectively occupy the entire control volume without any voids or overlaps. These equations are solved simultaneously for all three phases, along with momentum and energy conservation equations.

Momentum equation for the fluid phase where ($q=l$) [32]:

$$\nabla\cdot\left(\alpha_q\rho_q\vec{v}_q\vec{v}_q\right)=\alpha_q\nabla P+\nabla\cdot\bar{\bar{T}}_q+\alpha_q\rho_q\vec{g}+\sum_{p=1}^{n}\left(K_{pq}\left(\vec{v}_p-\vec{v}_q\right)+\dot{m}_{qp}\vec{v}_{pq}-\dot{m}_{qp}\vec{v}_{qp}\right)+\left(\vec{F}_q+\vec{F}_{\text{lift},q}+\vec{F}_{\text{vm},q}\right) \tag{3}$$

where $\vec{g}$ is the acceleration due to gravity, $\vec{F}_q$is an external body force, $\vec{F}_{\text{lift},q}$ is a lift force, $\vec{F}_{\text{vm},q}$ is a virtual mass force, and P is the pressure shared by all phases.

$\bar{\bar{\text{T}}}_q$ is the p^{th} phase stress-strain tensor, and be expressed as [32]:

$$\bar{\bar{\text{T}}}_q=\alpha_q\mu_q\left(\nabla\vec{v}_q+\nabla\vec{v}_q^{\,T}\right)+\alpha_q\left(\lambda_q-\frac{2}{3}\mu_q\right)\nabla\cdot\vec{v}_q\bar{\bar{I}} \tag{4}$$

$\lambda_q$and μ_q are the shear and bulk viscosity of phase q.

The fluid-solid exchange coefficient K_{pq}s can be written in the following general form, where = (s_1,s_2) and $q=l$ [32]:

$$K_{pq}=\frac{\alpha_p\rho_p f}{\tau_p} \tag{5}$$

where f is the drag function and τ_p, the "particulate relaxation time," is defined as [32]:

$$\tau_p=\frac{\rho_p d_p^2}{18\mu_l} \tag{6}$$

In this case = (s_1,s_2), d_p is the diameter of particles of phase (s_1,s_2)

The lift force $\vec{F}_{\text{lift}}$ acting on a secondary phase p in a primary phase q [32]:

$$\vec{F}_{\text{lift}}=-0.5\rho_q\alpha_p\left(\vec{v}_q-\vec{v}_p\right)\times\left(\nabla\times\vec{v}_q\right) \tag{7}$$

Momentum equation for solid phase [32]:

$$\nabla\cdot\left(\alpha_q\rho_q\vec{v}_q\vec{v}_q=\alpha_q\nabla P+\nabla\cdot\bar{\bar{T}}_q+\alpha_q\rho_q\vec{g}+\sum_{p=1}^{n}\left(K_{pq}\left(\vec{v}_p-\vec{v}_q\right)+\dot{m}_{qp}\vec{v}_{pq}-\dot{m}_{qp}\vec{v}_{qp}\right)+\left(\vec{F}_q+\vec{F}_{\text{lift},q}+\vec{F}_{\text{vm},q}\right)\right. \tag{8}$$

where q = (s_1,s_2), and n is the number of phases.

A separate enthalpy equation can be written for each phase to describe the conservation of energy in Eulerian multiphase applications [32]:

$$\nabla\cdot\left(\alpha_q\rho_q\vec{u}_q h_q\right)=\bar{\bar{T}}_q:\nabla\vec{u}_q-\nabla\cdot\left(k_q\nabla T_q\right)+\sum_{p=1}^{n}Q_{pq} \tag{9}$$

$k_q$and T_q represent the thermal conductivity and the temperature of each phase q = (l, s_1,s_2), respectively, and $Q_{pq}$is the intensity of heat exchange between the p^{th} and q^{th} phases.

The total specific enthalpy h_q can be expressed as follows for phase q = (l, s_2):

$$h_q=h_{\text{ref}}+\int_{T_{\text{ref}}}^{T_q}c_{p,q}\,dT \tag{10}$$

where h_{ref} is the reference enthalpy at the reference temperature T_{ref} , $c_{p,q}$ is the phase specific heat capacity.

For the solid phase q = (s_1), the total specific enthalpy of the MPCM particles can be calculated as follows:

$$h_q=h_{\text{ref}}+\int_{T_{\text{ref}}}^{T_q}c_{P,\text{MPCM}}(T)\,dT \tag{11}$$

where $c_{P,MPCM}(T)$ is the specific heat capacity of MPCM particles and can be expressed as follows:

$$c_{P,MPCM}(T) = \begin{cases} c_{P,s}, & (T_{MPCM} < T_s) \\ \frac{c_{P,s} + c_{P,l}}{2} + \frac{\Delta h}{T_l - T_s}, & (T_s \le T_{MPCM} \le T_l) \\ c_{P,l}, & (T_l < T_{MPCM}) \end{cases} \quad (12)$$

Δh represents the MPCM latent heat, and T_s and T_l are the solidus and liquidus temperatures of the PCM, respectively.

The energy equation of the solid layers (*SL*), shown in Fig. 1, can be expressed as:

$$\nabla \cdot (k_{SL} \nabla T_{SL}) + S_q = 0 \quad (13)$$

$k_{SL}$and$T_{SL}$are the thermal conductivity, and the temperature of the solid layers, respectively. S_q is a constant volumetric heat generation source term (W/m^3) applied to solid layers, equivalent to the amount of solar irradiation G ((W/m^2) absorbed by each layer, divided by the thickness of the layer (m).

The heat transfer at the interface can be computed using Fourier's law as follows:

$$k_i \frac{\partial T_i}{\partial N} = k_{i+1} \frac{\partial T_{i+1}}{\partial N} \quad (14)$$

where *i*represents any layer starting from the top layer (glass), i.e., the layer before the last one, $i + 1$ is the adjacent layer, N is the local coordinate normal to the interface.

At the start of the analysis, both the initial and ambient air temperatures are set to 34°C. The left and right walls of the PV module are treated as adiabatic due to their minimal contribution to heat exchange, given their significantly smaller surface area compared to the area exposed to solar radiation. The thermal collector's left wall is defined as a velocity inlet, while the right wall is specified as a pressure outlet. Table 2 presents the design parameters used in numerical investigations.

The following assumptions are made:

- The transmissivity of ethyl vinyl acetate (EVA) is approximately 100 %.
- There is no dust on the surface and solar irradiation G is uniform at 1000 W/m^2.
- The flow is steady, laminar, and incompressible.
- Temperature variation along the thickness is negligible.
- The thermal-physical properties of the solid layers, GO nanoparticles, and water are constant.
- The bottom side of the absorber duct is adiabatic.

Thermal and electrical efficiencies

The total thermal power absorbed by the coolant water and MPCM particles and GO nanoparticles, denoted as $E_{th,tot}$ is calculated as follows:

$$E_{th,tot} = E_{th,W} + E_{th,MPCM} + E_{th,GO} \quad (15)$$

where:

Table 2
Design parameters used in the numerical investigations [31,33,34],.

Parameter	Values
The length of the fluid duct	1350 mm
The fluid duct depth	30 mm
The length of the PV module	1570 mm
Transmissivity of glass	0.90
PV cell efficiency at standard test conditions	0.13
Absorptivity of solar cell	0.90
Solar Irradiation (G)	1000 W/m^2
Ambient temperature	34°C
Inlet velocity	0.0004–0.0007 m/s
Initial temperature	34°C

$$E_{th,W} = \dot{m}_l \, c_{p,l} \, (T_{out,l} - T_{in,l}) \quad (16)$$

$\dot{m}_l$ and $c_{p,l}$ represent the mass flow rate and specific heat capacity of the liquid phase (water), respectively. $T_{in}$and T_{out} denote the inlet and outlet temperature, respectively.

$$E_{th,MPCM} = \dot{m}_{s_1} \, c_{p,MPCM} \, (T_{out,s_1} - T_{in,s_1}) \quad (17)$$

where $\dot{m}_{s_1}$ and $c_{p,MPCM}$ represent the volume fraction, mass flow rate, and specific heat capacity of the solid phase (MPCM particles), respectively.

$$E_{th,GO} = \dot{m}_{s_2} \, c_{p,s_2} \, (T_{out,s_2} - T_{in,s_2}) \quad (18)$$

where $\dot{m}_{s_2}$ and c_{p,S_2} represent the volume fraction, mass flow rate, and specific heat capacity of the solid phase (GO nanoparticles), respectively.

The mass flow rate of each phase $q = (l, s_1, s_2)$ $\dot{m}_q$ is determined based on the phase density, phase velocity, and cross-sectional area of the channel, given by:

$$\dot{m}_q = \alpha_q \, \rho_q \, U_0 \, S_{ch} \quad (19)$$

where $\rho_q$is the density of the phase in kilograms per cubic meter (kg/m^3), U_0 represents the average velocity of the phase in meters per second (m/s), and S_{ch} is the cross-sectional area of the rectangular channel in square meters (m^2).

The thermal efficiency η_{th}can be calculated as follows:

$$\eta_{th} = \frac{E_{th,tot}}{G \, A_S} \quad (20)$$

where A_S is the surface area of the PV panel.

The electrical model describes how the efficiency of a PV cell is affected by temperature variations and can be determined using different formulations. The electrical efficiency (η_{el}) of a PV cell changes based on its operating temperature and is given by:

$$\eta_{el} = \eta_{ref} \left[1 - \beta_{ref} (T_c - T_{ref})\right] \quad (21)$$

where η_{el} is the electrical efficiency of the PV module at cell temperature T_c, η_{ref} is the reference efficiency at standard test conditions (STC), usually measured at solar irradiance of 1000 W/m^2, and reference temperature $T_{ref} = 25$°C. The term β_{ref} represents the thermal coefficient of efficiency loss, which depends on the PV module material, and for silicon cells, β_{ref}=0.0006/K [39]As the cell temperature increases, the efficiency of the PV module decreases due to increased resistance in the semiconductor material. This equation quantifies how much efficiency is lost per degree above the reference temperature.

The overall efficiency η_{tot} of the PVT system can be calculated as follows:

$$\eta_{tot} = \eta_{th} + \eta_{el} \quad (22)$$

2.3. Validation

The comparison between the numerical and Yamagishi et al. [35] experimental results for the thermal performance of the MPCM slurry and water is presented in Fig. 2 (a and b), respectively. As shown in the figures, the Yamagishi et al. [35] experimental results closely align with the numerical predictions, exhibiting minimal variation for both MPCM and water. For water, a linear relationship is observed between temperature and normalized depth, with experimental values consistently about 0.1°C higher than the numerical model. In contrast, the MPCM temperature follows a cubic trend with depth, where the experimental data closely matches the numerical model up to a normalized depth of 400. Beyond this point, a slight deviation is noted, with the experimental temperature being approximately 0.5°C higher than the numerical

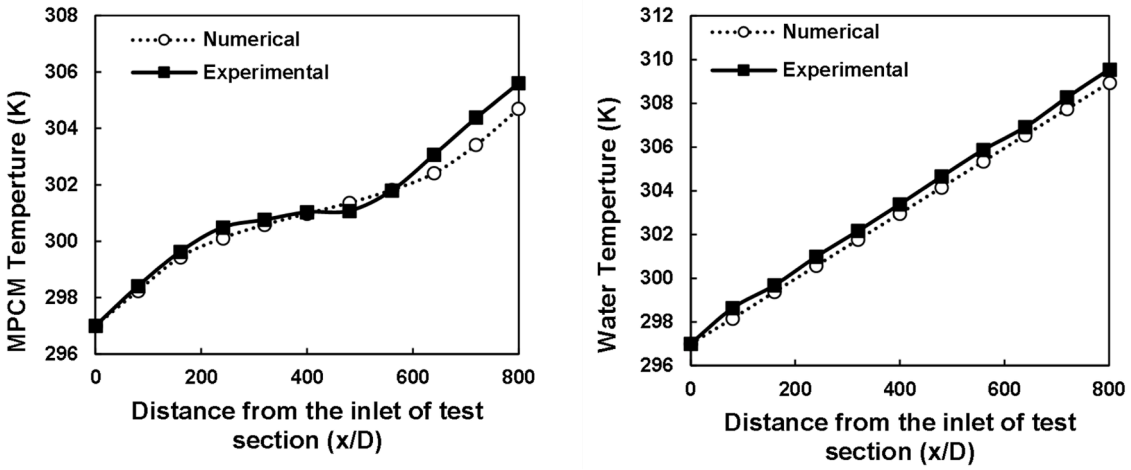


Fig. 2. Model validation for thermal performance of MPCM slurry and water.

predictions at a distance of 800 from the inlet of the test section (x/D). Despite these minor differences, the overall agreement between the experimental and numerical results validates the accuracy of the numerical model.

The effect of inlet velocity on average cell temperature, outlet temperature, electrical efficiency, and thermal efficiency is presented in Fig. 3 (a-d) respectively. The results from this study are compared with the experimental and numerical data reported by Nahar et al. [31]. Regarding average cell temperature, a general linear decrease is observed with increasing inlet velocity across all cases. At an inlet velocity of 0.0004 m/s, the average cell temperature in the present study is approximately 1°C lower than the experimental results of Nahar et al. [31]. This gap reduces progressively and disappears at an inlet velocity of 0.0007 m/s, where the temperature from the present study converges with the experimental results at around 61°C, which is 2.5°C higher than Nahar et al's numerical results at the same inlet velocity. Overall, across all inlet velocities, the present study shows better agreement with the experimental results of Nahar et al. than with their numerical results.

A similar trend is observed in the effect of inlet velocity on outlet temperature, where the outlet temperature decreases linearly with increasing inlet velocity. At an inlet velocity of 0.0004 m/s, the outlet temperatures from this study and Nahar et al.'s experimental results nearly overlap. However, as the inlet velocity increases, the results begin to diverge, reaching a maximum difference of approximately 2°C at an inlet velocity of 0.0007 m/s. Similar to the average cell temperature, the results from the present study align more closely with the experimental results of Nahar et al. [31] than with their numerical results across all inlet velocities.

For electrical efficiency, the trend suggests that it remains relatively unaffected by variations in inlet velocity, with a maximum increase of around 2 % reported in Nahar et al.'s numerical results as the inlet velocity rises from 0.0004 m/s to 0.0007 m/s. The results from the present study perfectly overlap with the experimental results of Nahar et al., both of which exhibit a consistent 2 % difference compared to Nahar et al.'s numerical data.

In the case of thermal efficiency, an overall decrease is observed with higher inlet velocities, although the rate of increase reported in both the experimental and numerical results of Nahar et al. is steeper than that in the present study. At an inlet velocity of 0.0004 m/s, the present study reports a thermal efficiency nearly 10 % higher than Nahar et al. [31]'s experimental results and is approximately 5 % higher than their numerical results. However, at an inlet velocity of 0.0007 m/s, the thermal efficiency in the present study converges with Nahar et al. [31]'s experimental results at around 68 %, which is approximately 5 % lower than the efficiency reported by Nahar et al. [31]'s numerical model.

3. Results

The proposed PVT system's thermal and electrical performance is analyzed using microencapsulated phase change material (MPCM) slurry as the working fluid. Performance evaluation is based on average PV cell temperature and overall efficiency, encompassing both thermal and electrical efficiencies. The research systematically investigates the effectiveness of MPCM slurry as a working fluid by analyzing volume fractions of 5 %, 10 %, and 15 % across melting temperatures of 35°C, 40°C, and 45°C. Water serves as the reference fluid, providing a benchmark for evaluating the thermal performance improvements achieved with MPCM slurry.

The configuration yielding the lowest average PV cell temperature and highest overall efficiency is identified as optimal. In the next phase, the study explores the effect of adding graphene oxide (GO) nanoparticles into the optimal configuration, evaluating its impact on PVT performance through key parameters: average PV cell temperature, thermal conductivity, pressure drop, overall efficiency, and temperature contour of the working fluid.

3.1. Influence of MPCM slurry melting temperature and inlet velocity on PVT system performance

The results for average cell temperature, outlet temperature, electrical efficiency, and thermal efficiency for the PVT panel using 5 % MPCM at 35°C, 40°C, and 45°C as working fluids are presented in Fig. 4 (a, b, c and d). respectively. Water was used as the control fluid for comparison. The data provides insights into the impact of working fluid temperature and flow rate on the thermal and electrical performance of the system.

Regarding average cell temperature, a general decrease was observed with lower working fluid temperatures across all cases. At 45°C, the average cell temperature closely matched the values obtained with water as the working fluid. At 40°C, the average cell temperature was consistently 0.75°C lower than at 45°C, while at 35°C, it showed an additional reduction of approximately 1°C. These results indicate that decreasing the MPCM temperature contributes to improved thermal regulation of the photovoltaic cells.

A similar trend is observed for outlet temperatures, where lower working fluid temperatures correspond to lower outlet temperatures. At a flow rate of 0.0004 m/s, the outlet temperatures for all three MPCM cases were nearly identical, around 48°C, which was approximately 2°C lower than the outlet temperature achieved with water. As the flow rate increased, the outlet temperatures for 5 % MPCM at 35°C and 40°C remained nearly identical, deviating by only 0.5°C at the maximum flow rate of 0.0007 m/s. In contrast, 5 % MPCM at 45°C consistently

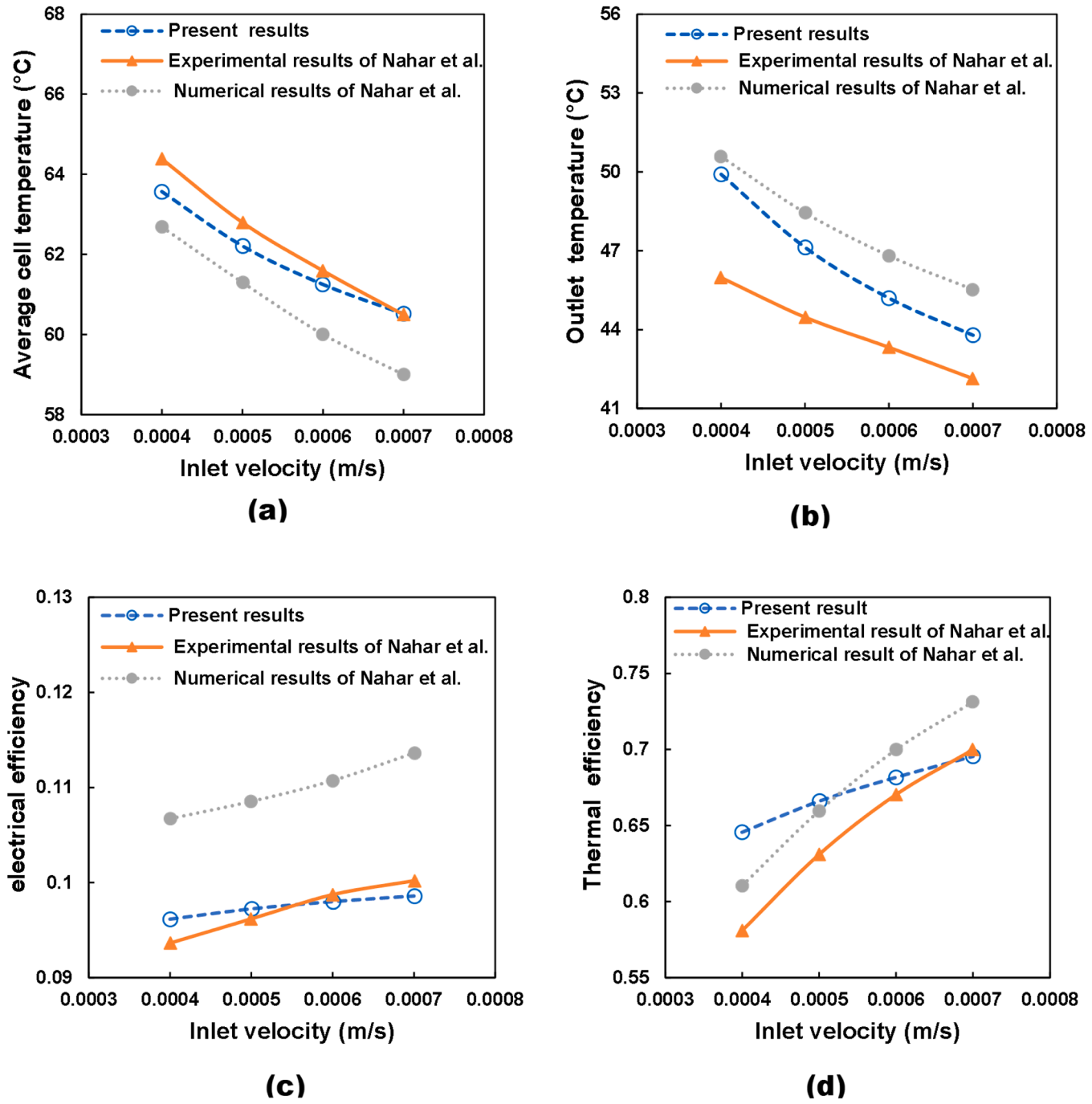


Fig. 3. Effect of inlet velocity on the performance of PV/T system using water as the working fluid.

produced higher outlet temperatures, reaching 44°C at 0.0007 m/s, a value overlapping with that obtained using water.

For electrical efficiency, a consistent increase with an increasing flow rate was observed across all cases. The highest electrical efficiency was reported by 5 % MPCM at 35°C, which was approximately 0.2 % higher than 5 % MPCM at 40°C and 0.4 % higher than the efficiency achieved using water. This trend highlights the advantage of using MPCM at lower temperatures to enhance the electrical performance of the system.

Thermal efficiency exhibited distinct trends depending on the working fluid temperature. For water and 5 % MPCM at 35°C, thermal efficiency increased linearly with flow rate, with water consistently producing thermal efficiency approximately 2 % higher than that of 5 % MPCM at 35°C across all flow rates. For 5 % MPCM at 40°C, thermal efficiency followed a nearly identical trend to that of water from 0.0004 m/s to 0.0005 m/s but showed a sharp rise thereafter, reaching a maximum value of 75 % at a flow rate of 0.0007 m/s, which was 10 % higher than the thermal efficiency at 0.0004 m/s. The thermal efficiency of 5 % MPCM at 45°C exhibited a unique behavior, increasing from 0.0004 m/s to 0.0005 m/s and peaking at 73 %, followed by a gradual decline to 70 % at the highest flow rate of 0.0007 m/s. This decrease can be attributed to the outlet temperature being lower than the PCM's melting point, preventing the absorption of latent heat during the process.

The overall efficiency, combining thermal and electrical efficiencies, demonstrated a strong correlation with flow rate. The relationship, however, varied with the working fluid. Water and 5 % MPCM at 35°C exhibited linear increases in overall efficiency with flow rate, while 5 % MPCM at 40°C and 45°C displayed nonlinear trends. The highest overall

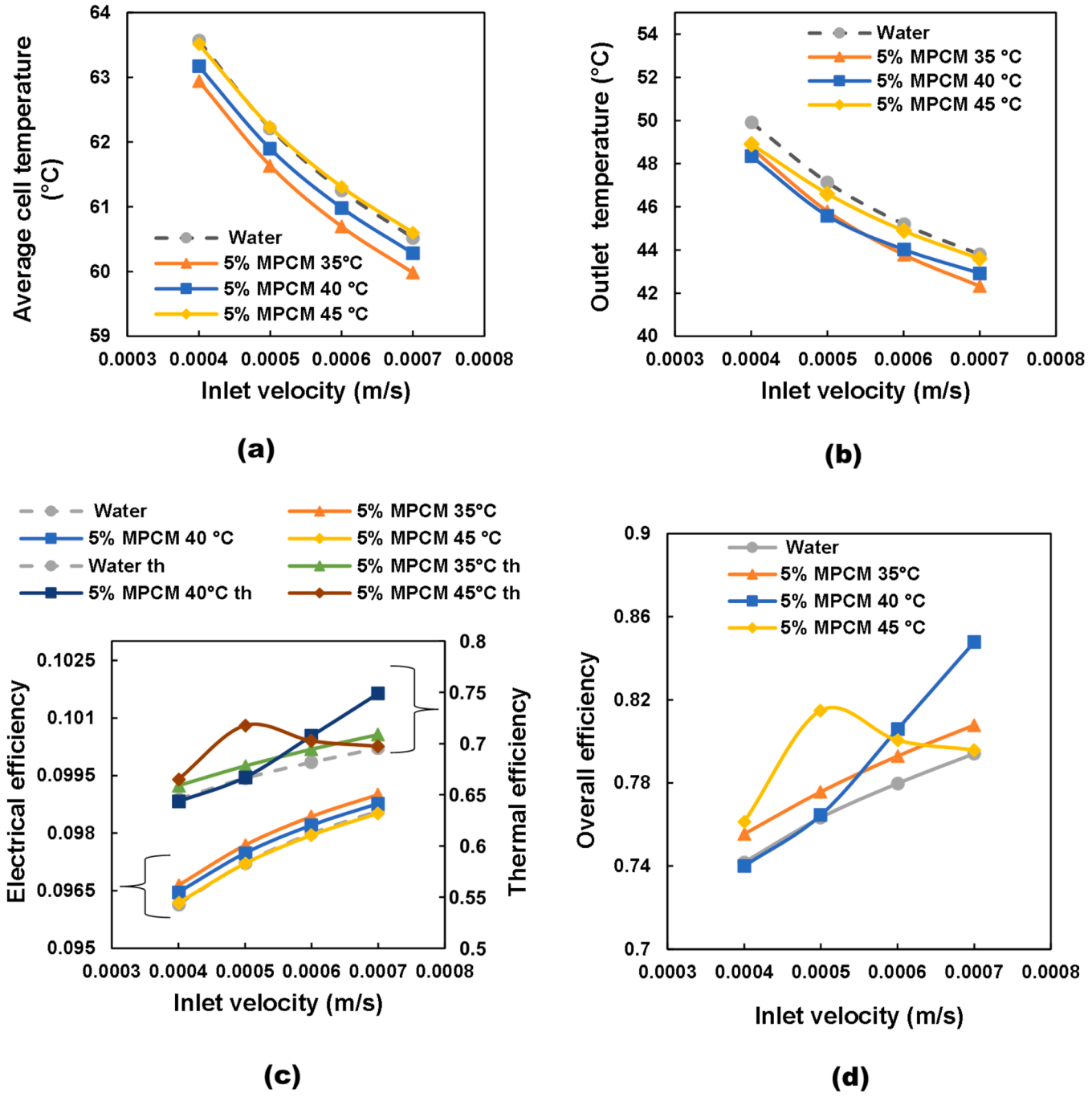


Fig. 4. Effect of melting temperature and inlet velocity of MPCM slurry on the performance of PVT system at 5 % MPCM volume fraction.

efficiency was reported for 5 % MPCM at 40°C at a flow rate of 0.0007 m/s, which was 10 % higher than the overall efficiency achieved with water at the same flow rate, and 6 % and 4 % higher than the maximum efficiencies reported for 5 % MPCM at 35°C and 45°C, respectively.

The results for average cell temperature, outlet temperature, electrical efficiency, and thermal efficiency for the PVT panel using 10 % MPCM at 35°C, 40°C, and 45°C as working fluids are presented in Fig. 5 (a-d), respectively. Water was used as the control fluid for comparison. Overall, the trends observed for the 10 % MPCM volume fraction closely resemble those reported for the 5 % MPCM case across all measurements, with notable improvements in thermal and electrical performance.

For average cell temperature, the results consistently show a reduction of approximately 1°C compared to the 5 % MPCM case across all samples tested. This reduction highlights the enhanced thermal regulation provided by the higher MPCM volume fraction. Similarly, the outlet temperature for 10 % MPCM is approximately 2°C lower across all working fluid temperatures compared to 5 % MPCM, further demonstrating improved heat absorption and transfer capabilities at the higher concentration.

In terms of overall efficiency, 10 % MPCM outperformed its 5 % counterpart in all cases. The highest overall efficiency was observed for 10 % MPCM at 40°C, reaching 93 %, which is 8 % higher than the maximum efficiency reported for 5 % MPCM at the same temperature and flow rate. Similar improvements were noted for 35°C and 45°C, where the maximum overall efficiencies were 5 % and 4 % higher, respectively, compared to their 5 % MPCM equivalents at identical flow rates.

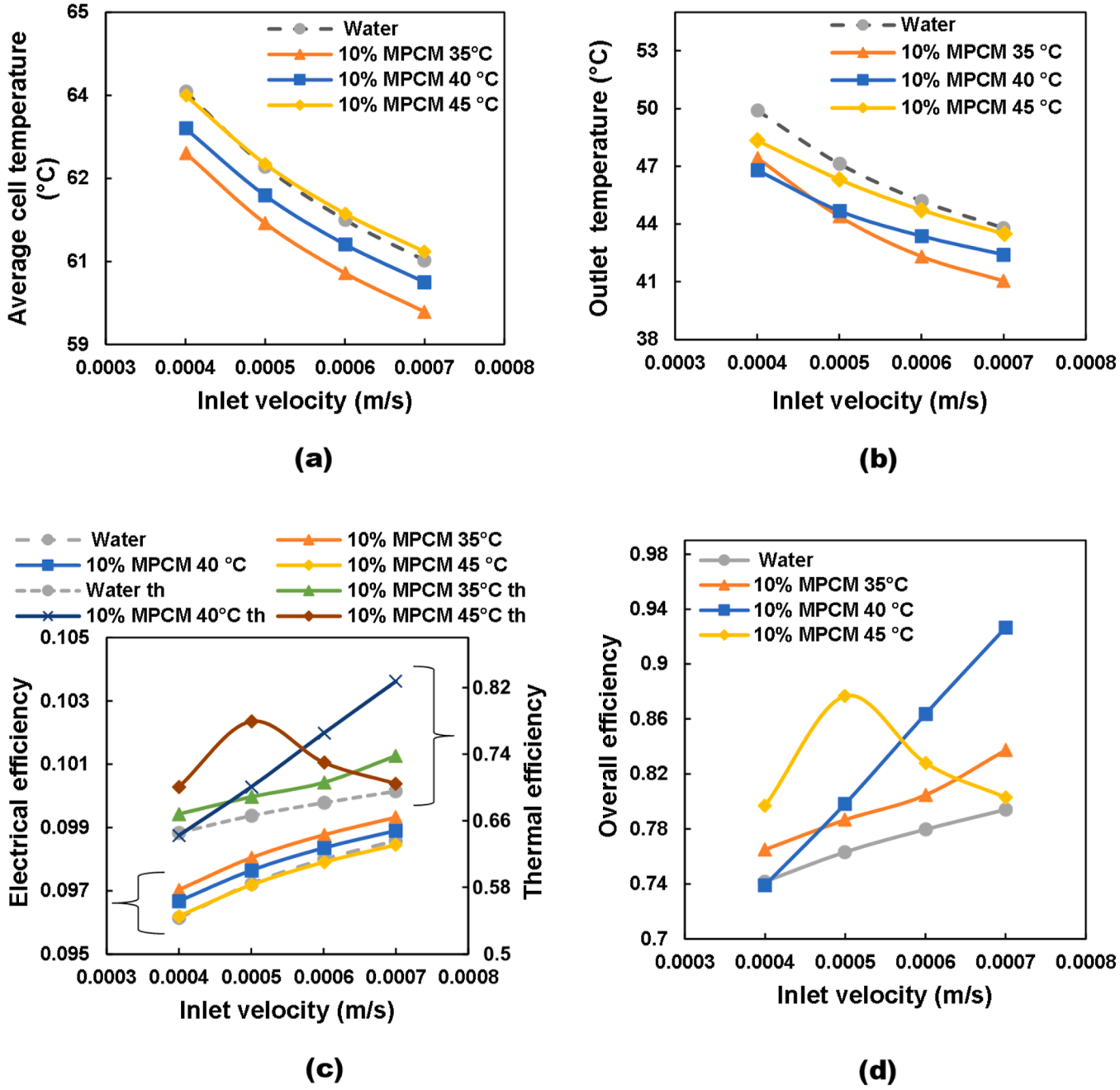


Fig. 5. Effect of melting temperature and inlet velocity of MPCM slurry on the performance of PVT system at 10 % MPCM volume fraction.

The results for the average cell temperature, outlet temperature, electrical efficiency, and thermal efficiency of the PVT panel using 15 % MPCM at 35°C, 40°C, and 45°C as working fluids are shown in Fig. 6 (a-d), respectively. Water served as the control fluid for comparison. Overall, the trends observed for the 15 % MPCM volume fraction closely align with those reported for the 5 % MPCM and 10 % MPCM cases across all measurements, with notable enhancements in both thermal and electrical performance.

For the average cell temperature, the results consistently indicate a reduction of about 1°C compared to the 5 % MPCM case across all samples tested and are nearly identical to those observed for the 10 % MPCM case. Similarly, the outlet temperature for 15 % MPCM is approximately 2°C lower across all working fluid temperatures compared to 5 % MPCM, while remaining similar to the 10 % MPCM case, further highlighting improved heat absorption and transfer capabilities at this higher concentration.

In terms of overall efficiency, the 15 % MPCM consistently outperformed the 5 % MPCM in all scenarios but fell short of the 10 % MPCM case. The highest overall efficiency for 15 % MPCM was recorded at 40°C, reaching 100 %, which is 7 % higher than the maximum efficiency reported for 10 % MPCM at the same temperature and flow rate. Similar efficiency improvements were observed at 35°C and 45°C, where the maximum overall efficiencies were 6 % and 5 % higher, respectively, compared to the 10 % MPCM equivalents at the same flow rates.

In conclusion, the results illustrate the impact of MPCM volume fraction, working fluid temperature, and flow rate on the performance of the PVT panel. Across all cases, MPCM consistently improved both thermal regulation and energy conversion efficiency compared to water. When comparing the three MPCM concentrations, higher fractions (10 % and 15 %) provided better heat absorption and transfer capabilities,

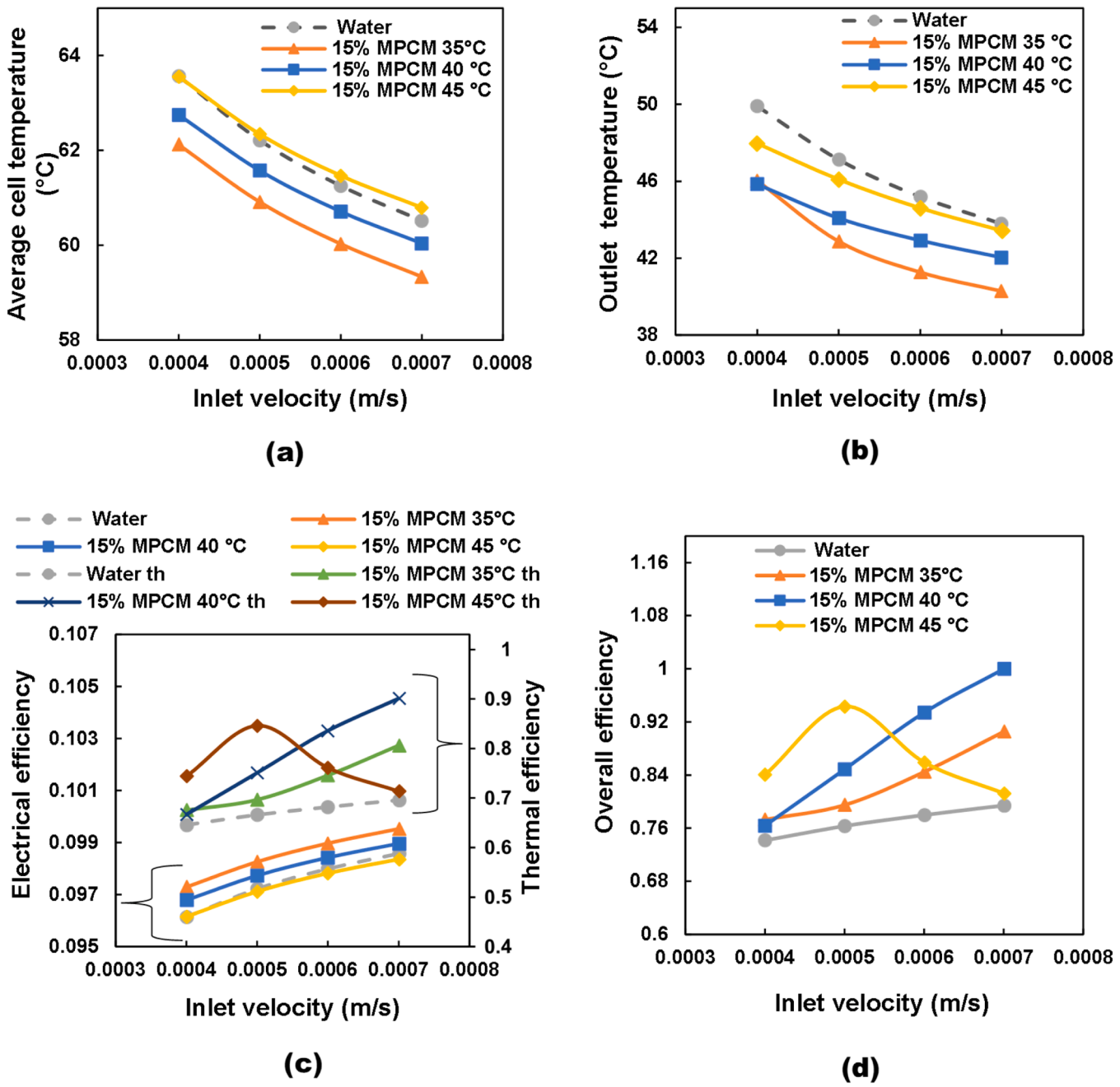


Fig. 6. Effect of melting temperature and inlet velocity of MPCM slurry on the performance of PVT system at 15 % MPCM volume fraction.

resulting in lower cell and outlet temperatures and improved overall efficiency. For example, the 10 % MPCM showed a clear advantage over the 5 % MPCM, with average cell temperatures approximately 1°C lower and outlet temperatures about 2°C lower across all working fluid temperatures. Similarly, 15 % MPCM further reduced these values while achieving higher overall efficiencies than 5 % MPCM in all cases.

At 40°C, 15 % MPCM achieved the highest recorded overall efficiency of 100 %, outperforming 10 % MPCM by 7 % and 5 % MPCM by 16 %. This trend was consistent at other working fluid temperatures, where 15 % MPCM showed incremental improvements over the lower fractions. However, while 15 % of MPCM excelled in thermal and electrical regulation, its overall efficiency at lower flow rates was closer to that of the 10 % MPCM, indicating diminishing returns at higher concentrations under certain conditions.

These results underscore the advantages of using MPCM-based systems, with higher concentrations providing significant performance gains while also highlighting the trade-offs associated with further increasing MPCM volume fractions. The findings provide a basis for optimizing MPCM concentrations and operating conditions in PVT systems to achieve higher energy efficiencies across varying temperatures and flow rates.

Fig. 7 (a-c) illustrates the effect of MPCM volume fraction and melting temperature on thermal, electrical, and overall efficiencies at an inlet velocity of 0.0007 m/s. As shown in the figure, the 15 % MPCM volume fraction achieves the highest thermal efficiency compared to the 5 % and 10 % fractions. The maximum thermal efficiency was recorded at 90 % for the 15 % MPCM at 40°C. Additionally, no significant difference in thermal efficiency was observed between the volume fractions at 45°C. The lowest thermal efficiency across all cases was reported at 35°C, while the highest was observed at 30°C.

For electrical efficiency, all cases exhibited nearly 10 % efficiency, indicating minimal variation with changes in MPCM concentration or

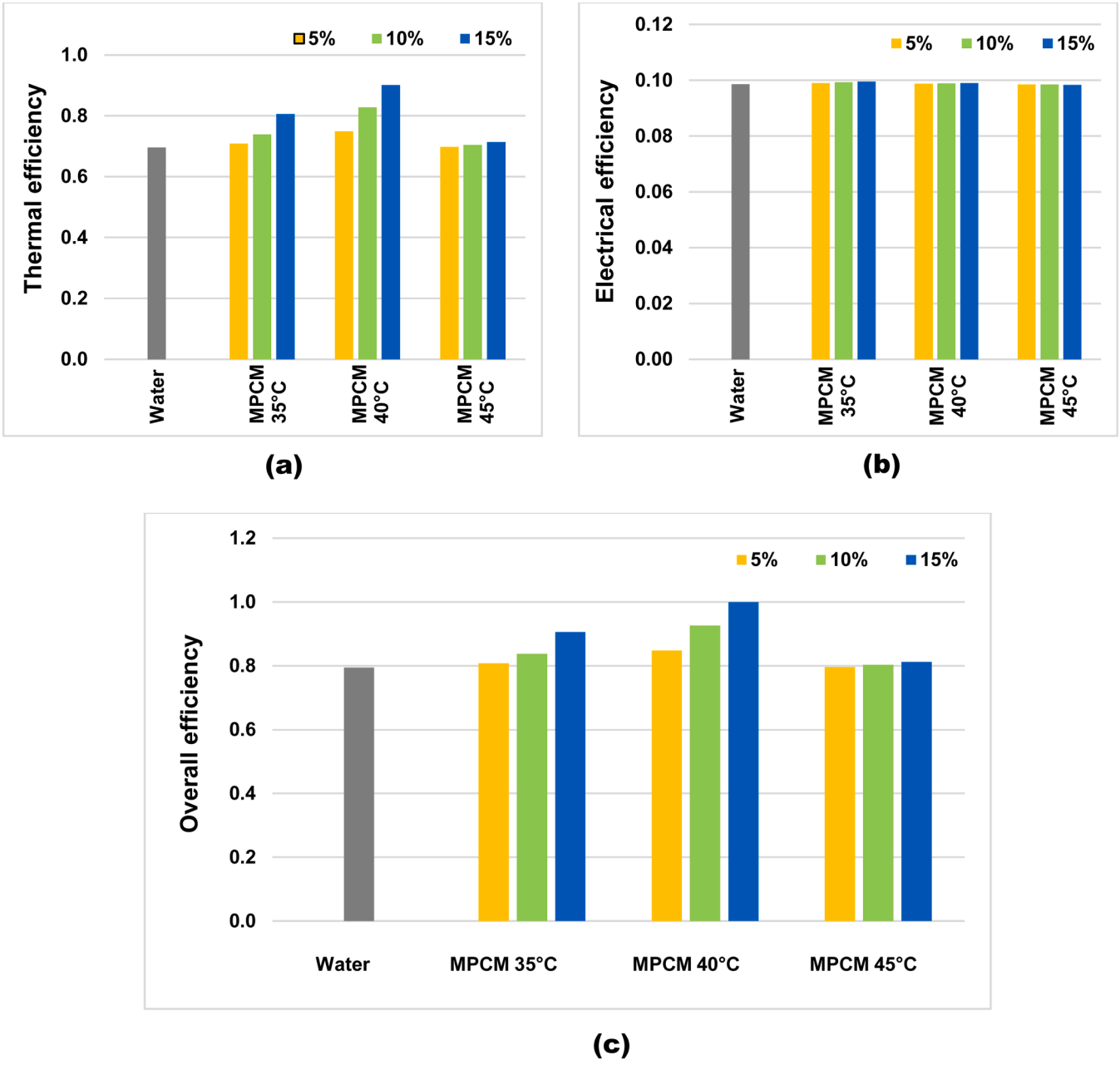


Fig. 7. Effect of MPCM volume fraction and melting temperature on the thermal, electrical and overall efficiencies of PV/T system at the inlet velocity of 0.0007 m/s.

temperature. Overall efficiency followed a trend similar to thermal efficiency, with 15 % MPCM at 40°C, reaching 10 %, the highest recorded value.

In general, the effect of temperature appears to be comparable to that of volume fraction. The increase in overall efficiency from 35°C to 40°C for the 15 % MPCM volume fraction was approximately 11 %, while the jump in efficiency at 40°C from 10 % to 15 % volume fraction was around 10 %. These results highlight the combined influence of MPCM concentration and temperature on system performance.

Fig. 8 illustrates the effect of MPCM melting temperature on the average fluid temperature distribution along the flow direction for a 15 % MPCM volume fraction at an inlet velocity of 0.0007 m/s, which appears to be the optimal case. As shown, the temperature increases nearly linearly along the flow direction. The results are compared against water as a control.

The temperature profile for 15 % MPCM at 45°C is nearly identical to that of water, indicating similar heat transfer characteristics. In contrast, the 40°C case follows a less steep temperature gradient, reaching a maximum temperature of 41°C at 1.5 m along the flow direction. The 35°C case exhibits an even flatter temperature profile, with a maximum temperature of approximately 39°C at 1.4 m. These trends suggest that lower melting temperatures lead to more gradual temperature increases along the flow path, influencing heat absorption and transfer dynamics.

3.2. Effect of adding graphene oxide (GO) to MPCM slurry on PVT system performance

Fig. 9 illustrates the effect of graphene oxide (GO) volume fraction and MPCM melting temperature on the outlet fluid temperature and the average temperature of the PV cell for a 15 % MPCM volume fraction at an inlet velocity of 0.0007 m/s.

For outlet temperature, a consistent 2°C difference is observed between the 40°C and 35°C cases, with the temperature decreasing slightly as the GO volume fraction increases. However, the reduction is minimal,

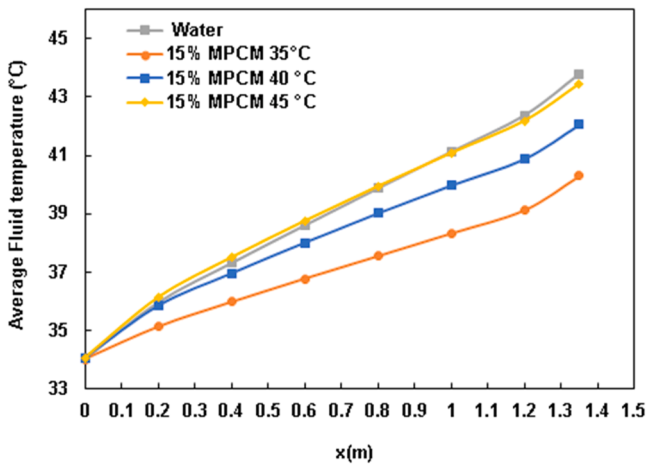


Fig. 8. Effect of MPCM melting temperature on the average fluid temperature distribution along the flow direction at the MPCM volume fraction of 0.15 and the inlet velocity of 0.0007 m/s.

with only a 0.5°C drop when the GO volume fraction increases from 0 to 0.02.

Regarding the average cell temperature, a steep decline is observed when the GO volume fraction increases from 0 to 0.005. Specifically, for the 15 % MPCM at 40°C, the temperature decreases by approximately 5°C, while for the 35°C case, the reduction is around 7°C. Beyond this point, further increases in GO volume fraction do not result in any significant changes in temperature.

Overall, the results indicate that while adding GO has a notable impact on thermal regulation, increasing its volume fraction beyond 0.005 does not produce further improvements in either outlet temperature or average cell temperature.

The temperature contours of different working fluids in the PVT system are illustrated in Fig. 10. The simulations consider an inlet velocity of 0.0007 m/s, with water, MPCM slurry (melting temperature of 40°C, volume fraction of 0.15), and nano-MPCM slurry containing GO nanoparticles at volume fractions of 0.5 %, 1.0 %, 1.5 %, and 2.0 %.

As the working fluid enters the channel at a lower temperature (blue) through the left inlet, it gradually heats up due to solar radiation applied to the top surface. This heating effect causes the upper region of the channel to shift toward red, reflecting an increase in temperature.

Water, serving as the baseline case, reaches the highest peak temperature of 56.1°C. Its temperature distribution exhibits a strong gradient from the hot upper surface to the cooler lower region. This suggests less effective heat transfer, as heat remains concentrated near the upper boundary rather than being evenly distributed downward.

On the other hand, using pure MPCM slurry as the working fluid results in poorer heat distribution, as indicated by the larger blue regions in the lower half of the channel. The low thermal conductivity of MPCM restricts heat transfer downward, causing more heat to be retained near the top. However, due to its high ability to absorb heat during melting at 40°C, the phase change effect helps regulate temperature, reducing the maximum temperature to 54.8°C.

The addition of GO nanoparticles significantly enhances heat transfer in the MPCM slurry due to GO's high thermal conductivity. This improvement is evident in the reduced blue regions at the bottom and the increased presence of green shades extending downward, indicating better thermal dissipation.

With increasing GO concentration, the thermal hotspot at the upper right edge gradually dissipates, as heat spreads leftward from the edge. Consequently, the maximum temperature drops from 46.9°C at 0.5 % GO to 45.4°C at 2.0 % GO.

However, beyond a certain concentration, the improvement becomes less pronounced: the temperature contours for 1.0 %, 1.5 %, and 2.0 % GO-MPCM slurries appear nearly identical. This suggests that increasing GO beyond 1.0–1.5 % has little additional effect. This plateauing could be attributed to factors beyond thermal conductivity, such as the heat transfer coefficient, flow rate, and the thermal resistance of PV module components (e.g., glass and backsheet). Furthermore, with an increase in the thermal conductivity of the fluid, the temperature difference between the PV cells and the fluid becomes smaller, and thus the driving force for heat transfer is minimized.

Fig. 11 shows the relationship between GO volume fraction, thermal conductivity and pressure drop for water, MPCM slurry, and GO-MPCM slurries used as working fluids in a PVT system. The MPCM slurry (0 % GO) exhibits the lowest thermal conductivity (0.55 W/m·K), even lower than that of water (0.60 W/m·K). However, with the addition of GO, thermal conductivity increases sharply, reaching 54.7 W/m·K at a 2.0 % GO concentration.

But with this improvement in thermal conductivity, pressure drop also increases, meaning more flow resistance. Pressure drop goes from 25.5 mPa (0 % GO) to 29.2 mPa (2.0 % GO), so higher viscosity of GO-MPCM Slurry leads to more frictional losses. This increased viscosity and flow resistance may require more pumping power which can negate some of the thermal performance benefits, especially in large scale applications where energy efficiency is crucial. So, GO enhances heat transfer but also changes the flow behavior in a way that can affect the

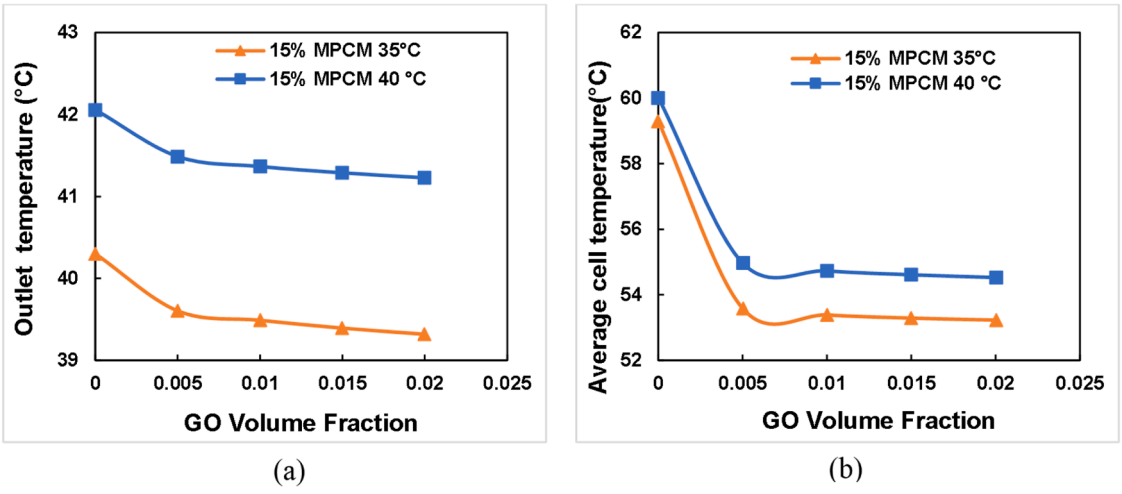


Fig. 9. Effect of graphene oxide (GO) volume fraction and MPCM melting temperature on the outlet fluid temperature and the average temperature of the PV cell at the MPCM volume fraction of 0.15 and the inlet velocity of 0.0007 m/s.

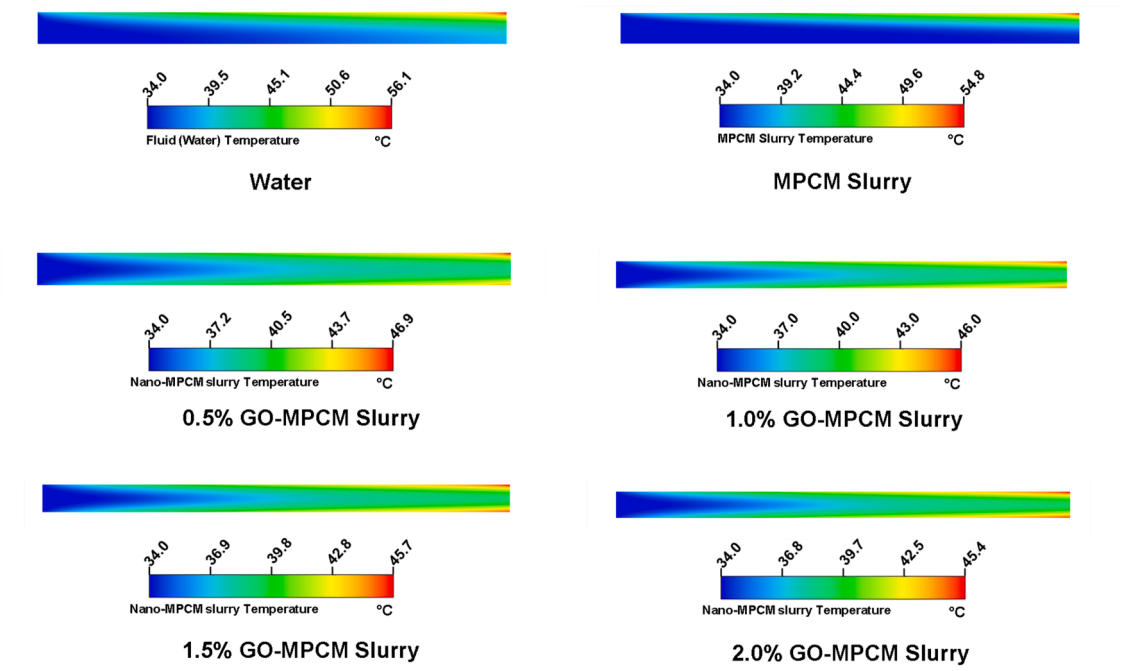


Fig. 10. Temperature contours of water, MPCM slurry, and GO-MPCM Slurries used as working fluids in a PVT system.

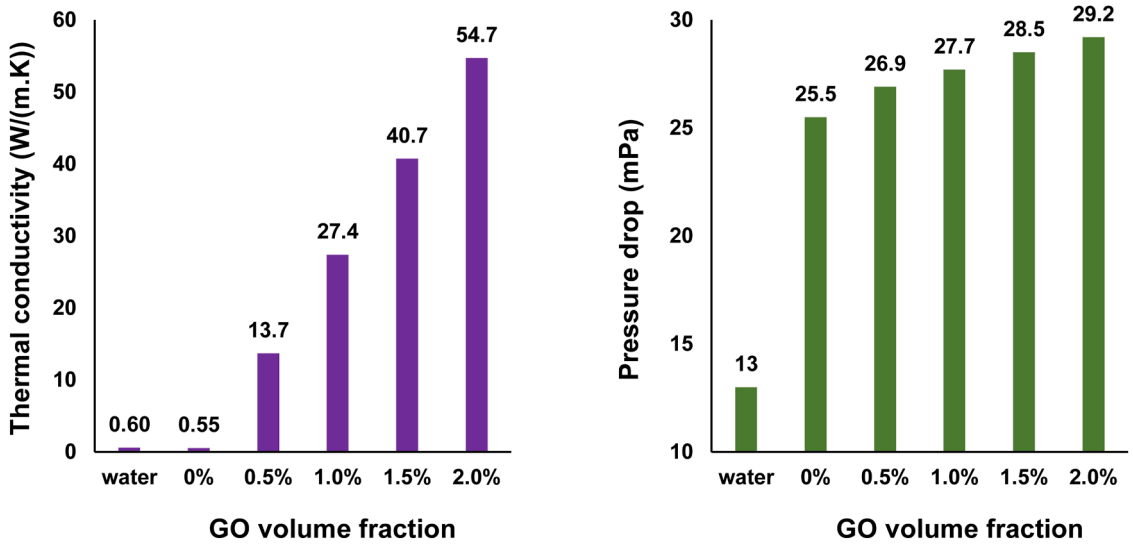


Fig. 11. Thermal conductivity and pressure drop values of water, MPCM slurry, and GO-MPCM slurries used as working fluids in a PVT system.

overall system performance.

The results suggest that the selection of GO concentration in MPCM slurries needs to be optimized carefully to balance heat transfer and pressure drop. Higher GO concentration increases thermal conductivity but also increases pumping power due to viscosity induced resistance. So, the ideal GO fraction should be chosen based on the PVT system requirements so that the thermal efficiency gain outweighs the energy cost of increased pressure drop.

Fig. 12a, b, and c illustrates the effect of graphene oxide (GO) volume fraction and MPCM melting temperature on thermal, electrical, and overall efficiency for a 15 % MPCM volume fraction at an inlet velocity of 0.0007 m/s.

For thermal efficiency, increasing the GO volume fraction resulted in a reduction for both the 35°C and 40°C cases, indicating that the addition of GO may slightly hinder thermal performance. In contrast, electrical efficiency showed an opposite trend, with GO increasing efficiency by approximately 4 % for the 35°C case and 3 % for the 40°C case. However, beyond a GO volume fraction of 0.005, no further improvements in electrical efficiency were observed.

When considering overall efficiency, the results suggest that the addition of GO does not provide significant benefits in any of the cases. While GO enhances electrical efficiency slightly, its negative impact on thermal efficiency offsets these gains, leading to minimal overall improvements.

Table 3 presents a comprehensive summary of the thermal and electrical performance of PVT systems across various configurations from previous studies and the current research. Notably, the highest thermal efficiency (90.1 %) is observed in the MPCM slurry-based system investigated in this study, surpassing previous studies on MPCM slurry implementations, which reported efficiencies between 73 % and 79.1 %. Similarly, the addition of GO nanoparticles to the MPCM slurry achieved 88.1 % thermal efficiency, maintaining strong performance

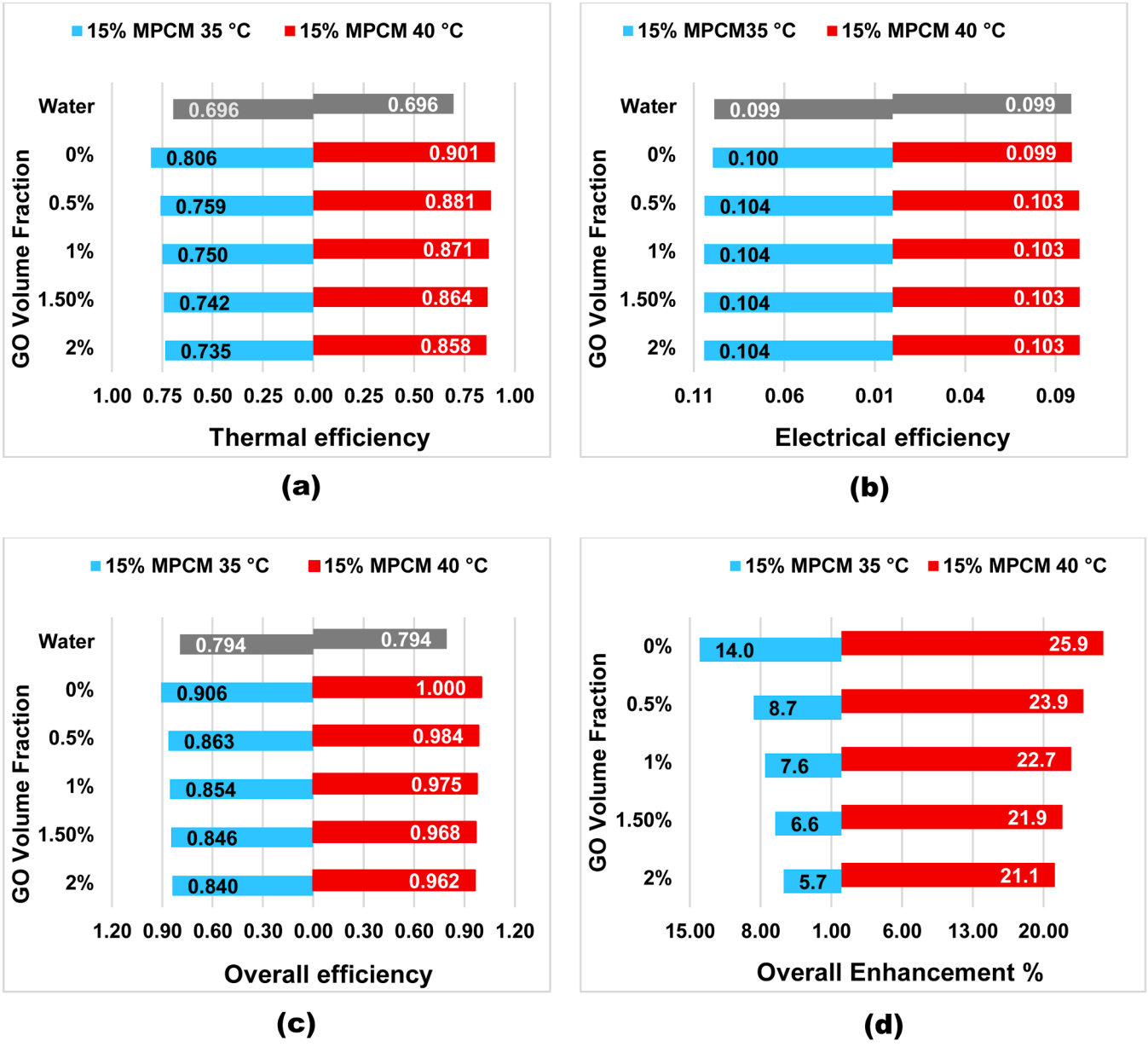


Fig. 12. Effect of graphene oxide (GO) volume fraction and MPCM melting temperature on the thermal, electrical and overall efficiencies of PVT system at the MPCM volume fraction of 0.15 and the inlet velocity of 0.0007 m/s.

relative to prior PCM-based studies. Additionally, the thermal efficiency of this study's system exceeds that of nanofluid-based PVT systems, which achieved efficiencies between 30.4 % and 80.2 % in previous studies.

A key distinction of this study's system is its semi-passive operation, where a pump is required only a few times a day to circulate the working fluid back to the tank. Unlike other PVT systems that rely on continuous pump operation for heat exchange, this system utilizes gravity-driven flow from the elevated tank to the PVT system, reducing energy consumption. It is important to note that variations in electrical efficiency values across different studies result from differences in PV models and types used.

Despite its various benefits, the deployment of nano-enhanced micro-encapsulated PCM slurry is not without obstacles. One of the key difficulties is the possibility for increased viscosity in the slurry owing to the inclusion of nanoparticles, which might alter the flow characteristics and need modifications in system design. Additionally, the expense of creating nano-enhanced MPCM slurry and the necessity for specialized equipment for their integration into slurry systems may provide economic problems. Ongoing research is focused on overcoming these difficulties by optimizing nanoparticle concentrations, enhancing synthesis procedures, and establishing cost-effective production processes [48].

For the proposed PVT system to be both cost-effective and practically feasible for real-world implementation, integrating it with emerging low-concentrating photovoltaic (CPV) technology would be advantageous. Researchers [49] at Stanford University recently developed a passive optical concentrator that eliminates the need for tracking systems and moving components. This technology concentrates sunlight onto solar cells regardless of the incident angle, capturing over 90 % of incoming radiation and forming output spots with threefold light intensity. Implementing this concentrator could reduce the number of required PVT units by a factor of three, resulting in savings of >50 % of the initial and maintenance costs.

Furthermore, recent advancements in anti-reflective coatings have significantly improved solar transmittance. Novel nanoarray structures

Table 3
A comparative thermal and electrical performances analysis of the current study and previous research on PVT systems.

No	Reference	System configuration with PVT	Finding(s)	
			Thermal efficiency	Electrical efficiency
1	[36]	Nano-enhanced PCM/ nanofluid	72 %	13.7 %
2	[37]	MPCM slurry	73 %	11.5 %
3	[38]	MPCM slurry	79.1 %	7.9 %
4	[39]	Dual-channel design – air and MPCM channels	71.8	8.9 %
5	[40]	PCM/nanofluid	~51 %	~14 %
6	[41]	Nanofluid	80.2 %	–
7	[42]	Water in wavy tubes	61.1 %	11.1 %
8	[42]	MPCM- silver nanoparticles slurry in wavy tubes	67.1 %	11.3 %
9	[43]	Hybrid nanofluids	30.4 %	18.5 %
10	[31]	Water	73.1 %	11.3 %
11	[44]	PVT collector with jet impingement	81 %	13.75 %
12	[45]	PCM	72.0 %	12.75 %
13	[46]	PCM	64.5 %	14.0 %
14	[47]	PCM	86.2	11.1 %
15	This study	MPCM slurry	90.1 %	9.9 %
16	This study	GO nanoparticles-MPCM slurry	88.1 %	10.3 %

[50] fabricated on glass covers exhibit exceptional anti-reflection properties across the 350–1100 nm wavelength range, achieving an average transmittance above 98 %, compared to conventional glass covers (90 %). Another study [51] demonstrated dip-coated antireflective nanostructured coatings with over 99 % transmittance in the 380–1600 nm range. These advancements will enhance optical transmission in PV and thermal components by reducing reflection losses. Additionally, they could improve the efficiency of passive optical concentrators, increasing their solar light capture from 90 % to approximately 98 %.

To prevent heat loss at high heat fluxes—particularly in cold seasons and under low-concentration solar conditions—without requiring an additional glass cover, a recently developed vacuum PV/T collector [52] should be considered. This design encloses both the upper and lower spaces of the PVT absorber in a vacuum environment. The top layer consists of a 10 mm thick glass cover that ensures high solar transmittance while minimizing heat dissipation.

While nano-MPCM slurry presents higher viscosity-induced resistance compared to water as a working fluid, the proposed system's semi-passive design counteracts this drawback by reducing energy consumption. The pump operates only a few times per day to return the working fluid to the elevated tank. In contrast to conventional PVT systems that rely on continuous pumping for heat exchange, this system utilizes the gravitational potential of the overhead reservoir tank to sustain circulation through the PVT collector, thereby enhancing operational efficiency.

For long-term slurry stability, a recent experimental study [30] demonstrated that GO nanoparticles significantly improve the dispersion stability of MPCM slurry compared to other nanoparticles and MPCM alone, reinforcing graphene's potential in advancing thermal management for PVT systems. To further stabilize the dispersion, sodium dodecyl sulfate (SDS) was employed as a surfactant, exhibiting proven effectiveness in GO nanofluids, and MPCMs [30]. Moreover, periodic circulation of the nano-MPCM slurry via a pump ensures continuous nanoparticle suspension, effectively reducing the risks of sedimentation and agglomeration.

The proposed PVT system, incorporating a passive optical concentrator, anti-reflective coatings, and a vacuum chamber, offers superior economic viability compared to typical PVT systems. The passive concentrator increases light intensity without tracking, reducing the required number of PVT units by up to three times, significantly lowering both installation and maintenance costs. Anti-reflective coatings enhance solar absorption, improving efficiency without additional material costs. Meanwhile, the vacuum chamber minimizes heat loss, maximizing thermal output and reducing reliance on external energy sources, making the system more cost-effective in the long run.

The proposed PVT system offers a significant environmental advantage over traditional fossil-fuel-based boilers commonly used in industrial applications. Conventional boilers burn natural gas, coal, or oil, releasing large quantities of CO_2 and contributing to global warming. In contrast, the PVT-powered system uses renewable solar energy to supply electrical heating and preheat water entering the boiler, reducing greenhouse gas emissions. Additionally, improved heat transfer efficiency minimizes energy waste, further decreasing the reliance on fossil fuels.

4. Conclusion

This study presents a novel approach to enhancing the performance of photovoltaic/thermal (PVT) systems by integrating a nano-enhanced microencapsulated phase change material (MPCM) slurry. The incorporation of graphene oxide (GO) nanoparticles effectively improves the dispersion stability of the MPCM slurry and significantly increases its thermal conductivity, thus optimizing the heat removal process from the photovoltaic cells. Additionally, the system's semi-passive design reduces energy consumption by limiting pump usage. A numerical evaluation identifies the optimal MPCM configuration, followed by an assessment of GO's impact on performance.

The key findings of this study include:

- Increasing MPCM volume fraction from 5 % to 15 % improves overall efficiency by up to 16 %, with the highest efficiency of 100 % observed at 15 % MPCM.
- The addition of GO nanoparticles, with a volume fraction of just 0.5 %, to the MPCM slurry reduces PV cell temperatures by up to 5°C at 40°C MPCM melting point.
- Thermal conductivity of the MPCM slurry (0 % GO) is 0.55 W/m·K, lower than water (0.60 W/m·K), but increases to 54.7 W/m·K at 2.0 % GO. However, this also raises the pressure drop from 25.5 mPa to 29.2 mPa, increasing flow resistance.
- Temperature contours reveal that using water as working fluid reaches the highest peak temperature (56.1°C), while nano-MPCM slurry enhances heat dissipation, lowering peak temperatures and spreading heat more evenly.
- The optimization of GO concentration is crucial, as excessive GO increases viscosity and pumping power requirements.
- A 15 % MPCM volume fraction with a melting point of 40°C yields the highest thermal efficiency of 90.1 %, outperforming water by 20.1 % and surpassing previous studies on MPCM slurries and nanofluids.

To make the proposed PVT system cost-effective and feasible for real-world implementation, three key technologies should be integrated. A passive optical concentrator eliminates the need for tracking systems while increasing light intensity, reducing the number of required PVT units and cutting costs. Advanced anti-reflective coatings enhance solar transmittance, minimizing reflection losses and boosting efficiency. Additionally, a vacuum chamber between the glass and PV cell significantly reduces heat loss, improving thermal performance, particularly in cold conditions or under low solar concentration.

Future research could focus on enhancing heat transfer performance and electrical efficiency in PVT systems by incorporating fins into the fluid channel or exploring microchannel designs. Additionally, investigating alternative PCM compositions, such as bio-based PCMs or eutectic mixtures, may offer improved thermal performance and greater

sustainability benefits. Another promising direction involves developing machine learning algorithms to predict PV temperature and thermal efficiency, enabling the identification of optimal working fluid configurations under varying environmental conditions, including solar radiation, wind speed, and ambient temperature.

Declaration of generative AI and AI-assisted technologies in the writing process

In the preparation of this manuscript, the authors employed ChatGPT to assist with proofreading and improving readability and language clarity. After utilizing this tool, the authors carefully reviewed and edited the content as necessary and take full responsibility for the final published version.

CRediT authorship contribution statement

Ahmed Azmeer: Writing – review & editing, Writing – original draft, Formal analysis. **Yahya Sheikh:** Validation, Software, Methodology, Data curation, Conceptualization. **Hasan A. Kanjo:** Writing – review & editing, Writing – original draft, Supervision. **Hamzeh Sabouni:** Writing – review & editing, Writing – original draft.

Declaration of competing interest

The authors declare that they have no known competing financial interests or personal relationships that could have appeared to influence the work reported in this paper.

Data availability

Data will be made available on request.

References

[1] Y. Sheikh, M. Jasim, M. Qasim, A. Qaisieh, M.O. Hamdan, F. Abed, Enhancing PV solar panel efficiency through integration with a passive Multi-layered PCMs cooling system: a numerical study, Int. J. Thermofluids 23 (2024) 100748, https://doi.org/10.1016/J.IJFT.2024.100748.

[2] H. Madhi, S. Aljabair, A.A. Imran, A review of photovoltaic/thermal system cooled using mono and hybrid nanofluids, Int. J. Thermofluids 22 (2024) 100679, https://doi.org/10.1016/J.IJFT.2024.100679.

[3] P. Saini, V. Kivioja, L. Naskali, J. Byström, C. Semeraro, A. Gambardella, X. Zhang, Techno-economic assessment of a novel hybrid system of solar thermal and photovoltaic driven sand storage for sustainable industrial steam production, Energy Convers. Manage. 292 (2023) 117414, https://doi.org/10.1016/J.ENCONMAN.2023.117414.

[4] K.Ibn Batouta, S. Aouhassi, K. Mansouri, Sustainable energy transition: a steam system optimization case study from a Moroccan food industry, Results. Eng. 24 (2024) 102944, https://doi.org/10.1016/J.RINENG.2024.102944.

[5] Introduction to electrified steam in food and beverage manufacturing, (n.d.). https://www.spiraxsarco.com/global/en-GB/news/introduction-to-electrified-steam-in-food-and-beverage-manufacturing (accessed January 31, 2025).

[6] L. Xu, L. Pu, S. Zhang, Z. Ma, Thermo-fluidic performance of microencapsulated phase change material slurry in thermal energy storage, J. Energy Storage 43 (2021) 103247, https://doi.org/10.1016/J.EST.2021.103247.

[7] O.A. Balogun, Y. Sun, P.A. Gbadega, Coordination of smart inverter-enabled distributed energy resources for optimal PV-BESS integration and voltage stability in modern power distribution networks: a systematic review and bibliometric analysis, E-Prime - Adv. Electr. Eng. Electron. Energy 10 (2024) 100800, https://doi.org/10.1016/J.PRIME.2024.100800.

[8] A. Dashtbozorg, B. Safarianbana, M. Shanbedi, Enhancing PV/T systems performance: a comprehensive study on MXene/methanol nanofluid in two-phase closed thermosyphons, Solar Energy Mater. Solar Cells 279 (2025) 113274, https://doi.org/10.1016/J.SOLMAT.2024.113274.

[9] P. Saini, V. Kivioja, L. Naskali, J. Byström, C. Semeraro, A. Gambardella, X. Zhang, Techno-economic assessment of a novel hybrid system of solar thermal and photovoltaic driven sand storage for sustainable industrial steam production, Energy Convers. Manage. 292 (2023) 117414, https://doi.org/10.1016/J.ENCONMAN.2023.117414.

[10] G. Saha, A.A.M. Azad, A review of advancements in solar PV-powered refrigeration: enhancing efficiency, sustainability, and operational optimization, Energy Rep. 12 (2024) 1693–1709, https://doi.org/10.1016/J.EGYR.2024.07.046.

[11] M.M. Abdel-Aziz, A.Elnaby Kabeel, A. Khelifa, M. El Hadi Attia, M. Bady, A numerical investigation on improving the thermal efficiency of PV panels through integration with solar water collectors, Solar Energy 287 (2025) 113259, https://doi.org/10.1016/J.SOLENER.2025.113259.

[12] J. Liu, C. Peng, J. Zhang, Understanding the relationship between rural morphology and photovoltaic (PV) potential in traditional and non-traditional building clusters using shapley additive exPlanations (SHAP) values, Appl. Energy 380 (2025) 125091, https://doi.org/10.1016/J.APENERGY.2024.125091.

[13] S.K. Saha, Empowering rural South Asia: off-grid solar PV, electricity accessibility, and sustainable agriculture, Appl. Energy 377 (2025) 124639, https://doi.org/10.1016/J.APENERGY.2024.124639.

[14] K. Sun, Y. Jiang, H. Liu, Configuration optimization of PV array for stratospheric airship under nonuniform radiation condition, Aerosp. Sci. Technol. 155 (2024) 109550, https://doi.org/10.1016/J.AST.2024.109550.

[15] A. Galimshina, J. McCarty, C. Waibel, A. Schlueter, A. Hollberg, High-resolution parametric embodied impact configurator for PV and BIPV systems, Renew. Energy 236 (2024) 121404, https://doi.org/10.1016/J.RENENE.2024.121404.

[16] Y. Sheikh, M.F. Orhan, M. Kanoglu, M. Umair, E. Mehaisi, Effect on the thermal performance of a bio-based phase change material with the addition of graphite with surfactants, Heat Transf. Eng. 45 (2024) 765–778, https://doi.org/10.1080/01457632.2023.2220473.

[17] Y. Sheikh, M.F. Orhan, M. Umair, E. Mehaisi, A. Azmeer, Variation in cooling performance of a bio-based phase change material by adding graphene nanoplatelets with surfactants, Int. J. Thermofluids 16 (2022) 100201, https://doi.org/10.1016/J.IJFT.2022.100201.

[18] H. Shakibi, S. Afzal, A. Shokri, B. Sobhani, Utilization of a phase change material with metal foam for the performance improvement of the photovoltaic cells, J. Energy Storage 51 (2022) 104466, https://doi.org/10.1016/J.EST.2022.104466.

[19] Y. Sheikh, M.F. Orhan, A. Azmeer, Melting performance of a composite bio-based phase change material: an experimental evaluation of copper foam pore size, Int. J. Thermofluids 16 (2022) 100216, https://doi.org/10.1016/J.IJFT.2022.100216.

[20] Y. Sheikh, M.O. Hamdan, S. Sakhi, A review on micro-encapsulated phase change materials (EPCM) used for thermal management and energy storage systems: fundamentals, materials, synthesis and applications, J. Energy Storage 72 (2023) 108472, https://doi.org/10.1016/J.EST.2023.108472.

[21] A. Djalab, Z. Djalab, A. El Hammoumi, G. Marco TINA, S. Motahhir, A.A. Laouid, A comprehensive review of floating photovoltaic systems: tech advances, marine environmental influences on offshore PV systems, and economic feasibility analysis, Solar Energy 277 (2024) 112711, https://doi.org/10.1016/J.SOLENER.2024.112711.

[22] S.D. Prasetyo, Z. Arifin, A.R. Prabowo, E.P. Budiana, Investigation of the addition of fins in the collector of water/Al2O3-based PV/T system: validation of 3D CFD with experimental study, Case Stud. Therm. Eng. 60 (2024) 104682, https://doi.org/10.1016/J.CSITE.2024.104682.

[23] N. Yang, Q. Liu, B. Wang, J. Xuan, L. Xing, A novel PV/T system integrated with spectral beam filter: a comprehensive optical and thermodynamic study, Appl. Therm. Eng. 257 (2024), https://doi.org/10.1016/j.applthermaleng.2024.124457.

[24] H. Madhi, S. Aljabair, A.A. Imran, Comparative numerical study on the effect of fin orientation on the photovoltaic/thermal (PV/T) system performance, Int. J. Thermofluids 24 (2024), https://doi.org/10.1016/j.ijft.2024.100909.

[25] A. Khelifa, A.E. Kabeel, M.E.H. Attia, M. Abdelgaied, M. Arıcı, M.M. Abdel-Aziz, 3D numerical analysis of a photovoltaic thermal using bi-fluid: Al_2O_3–water nanofluid at various concentrations, Int. J. Thermofluids 20 (2023), https://doi.org/10.1016/j.ijft.2023.100523.

[26] C. Ould-Lahoucine, H. Ramdani, D. Zied, Energy and exergy performances of a TiO2-water nanofluid-based hybrid photovoltaic/thermal collector and a proposed new method to determine the optimal height of the rectangular cooling channel, Solar Energy 221 (2021) 292–306, https://doi.org/10.1016/J.SOLENER.2021.04.027.

[27] H. Ijaz, H. Raza, G.A. Gohar, S. Ullah, A. Akhtar, M. Imran, Effect of graphene oxide doped nano coolant on temperature drop across the tube length and effectiveness of car radiator – A CFD study, Therm. Sci. Eng. Prog. 20 (2020) 100689, https://doi.org/10.1016/J.TSEP.2020.100689.

[28] S. Ghosh, I. Calizo, D. Teweldebrhan, E.P. Pokatilov, D.L. Nika, A.A. Balandin, W. Bao, F. Miao, C.N. Lau, Extremely high thermal conductivity of graphene: prospects for thermal management applications in nanoelectronic circuits, Appl. Phys. Lett. 92 (2008), https://doi.org/10.1063/1.2907977/325960.

[29] L. Yudong, W. Jiangqing, S. Chuangjian, G. Shichao, G. Yongkun, P. Quangui, Nucleation rate and supercooling degree of water-based graphene oxide nanofluids, Appl. Therm. Eng. 115 (2017) 1226–1236, https://doi.org/10.1016/J.APPLTHERMALENG.2016.10.051.

[30] S. Mo, J. Ye, L. Jia, Y. Chen, Properties and performance of hybrid suspensions of MPCM/nanoparticles for LED thermal management, Energy 239 (2022) 122650, https://doi.org/10.1016/J.ENERGY.2021.122650.

[31] A. Nahar, M. Hasanuzzaman, N.A. Rahim, Numerical and experimental investigation on the performance of a photovoltaic thermal collector with parallel plate flow channel under different operating conditions in Malaysia, Solar Energy 144 (2017) 517–528, https://doi.org/10.1016/J.SOLENER.2017.01.041.

[32] A. Fluent, Ansys fluent theory guide, USA 15317 (2011) 724–746.

[33] I. Ceylan, A.E. Gürel, H. Demircan, B. Aksu, Cooling of a photovoltaic module with temperature controlled solar collector, Energy Build. 72 (2014) 96–101, https://doi.org/10.1016/J.ENBUILD.2013.12.058.

[34] S. Dubey, A.A.O. Tay, Testing of two different types of photovoltaic–thermal (PVT) modules with heat flow pattern under tropical climatic conditions, Energy Sustain. Develop. 17 (2013) 1–12, https://doi.org/10.1016/J.ESD.2012.09.001.

[35] Y. Yamagishi, H. Takeuchi, A.T. Pyatenko, N. Kayukawa, Characteristics of microencapsulated PCM slurry as a heat-transfer fluid, AIChE J. 45 (1999) 696–707, https://doi.org/10.1002/AIC.690450405.
[36] A.H.A. Al-Waeli, K. Sopian, M.T. Chaichan, H.A. Kazem, A. Ibrahim, S. Mat, M. H. Ruslan, Evaluation of the nanofluid and nano-PCM based photovoltaic thermal (PVT) system: an experimental study, Energy Convers. Manage. 151 (2017) 693–708, https://doi.org/10.1016/J.ENCONMAN.2017.09.032.
[37] Q. Yu, A. Romagnoli, R. Yang, D. Xie, C. Liu, Y. Ding, Y. Li, Numerical study on energy and exergy performances of a microencapsulated phase change material slurry based photovoltaic/thermal module, Energy Convers. Manage. 183 (2019) 708–720, https://doi.org/10.1016/J.ENCONMAN.2019.01.029.
[38] G. Wei, Y. Xiao, M. Sherin, L. Cui, X. Du, Numerical study on electrical and thermal performance of a novel concentrated photovoltaic/thermal system, Appl. Therm. Eng. 244 (2024) 122647, https://doi.org/10.1016/J.APPLTHERMALENG.2024.122647.
[39] L. Liu, Y. Jia, Y. Lin, G. Alva, G. Fang, Performance evaluation of a novel solar photovoltaic–thermal collector with dual channel using microencapsulated phase change slurry as cooling fluid, Energy Convers. Manage. 145 (2017) 30–40, https://doi.org/10.1016/J.ENCONMAN.2017.04.089.
[40] M. Hosseinzadeh, M. Sardarabadi, M. Passandideh-Fard, Energy and exergy analysis of nanofluid based photovoltaic thermal system integrated with phase change material, Energy 147 (2018) 636–647, https://doi.org/10.1016/J.ENERGY.2018.01.073.
[41] L. Sahota, G.N.Tiwari Shyam, Analytical characteristic equation of nanofluid loaded active double slope solar still coupled with helically coiled heat exchanger, Energy Convers. Manage. 135 (2017) 308–326, https://doi.org/10.1016/J.ENCONMAN.2016.12.078.
[42] M. Eisapour, A.H. Eisapour, M.J. Hosseini, P. Talebizadehsardari, Exergy and energy analysis of wavy tubes photovoltaic-thermal systems using microencapsulated PCM nano-slurry coolant fluid, Appl. Energy 266 (2020) 114849, https://doi.org/10.1016/J.APENERGY.2020.114849.
[43] R. Sathyamurthy, A.E. Kabeel, A. Chamkha, A. Karthick, A. Muthu Manokar, M. G. Sumithra, Experimental investigation on cooling the photovoltaic panel using hybrid nanofluids, Appl. Nanosci. (Switzerland) 11 (2021) 363–374, https://doi.org/10.1007/S13204-020-01598-2/FIGURES/11.
[44] A.H. Jaaz, K. Sopian, T.S. Gaaz, Study of the electrical and thermal performances of photovoltaic thermal collector-compound parabolic concentrated, Results. Phys. 9 (2018) 500–510, https://doi.org/10.1016/J.RINP.2018.03.004.
[45] H. Fayaz, N.A. Rahim, M. Hasanuzzaman, R. Nasrin, A. Rivai, Numerical and experimental investigation of the effect of operating conditions on performance of PVT and PVT-PCM, Renew. Energy 143 (2019) 827–841, https://doi.org/10.1016/J.RENENE.2019.05.041.
[46] S. Alsaqoor, A. Alqatamin, A. Alahmer, Z. Nan, Y. Al-Husban, H. Jouhara, The impact of phase change material on photovoltaic thermal (PVT) systems: a numerical study, Int. J. Thermofluids 18 (2023) 100365, https://doi.org/10.1016/J.IJFT.2023.100365.
[47] M.S. Hossain, L. Kumar, A. Arshad, J. Selvaraj, A.K. Pandey, N.A. Rahim, A comparative investigation on solar PVT- and PVT-PCM-based collector constancy performance, Energies. (Basel) 16 (2023) 2224, https://doi.org/10.3390/EN16052224, 2023Page 2224 16.
[48] A. Allouhi, S. Rehman, M.S. Buker, Z. Said, Recent technical approaches for improving energy efficiency and sustainability of PV and PV-T systems: a comprehensive review, Sustain. Energy Technol. Assess. 56 (2023) 103026, https://doi.org/10.1016/J.SETA.2023.103026.
[49] N. Vaidya, O. Solgaard, Immersion graded index optics: theory, design, and prototypes, Microsyst. Nanoeng. 8 (2022) 1–11, https://doi.org/10.1038/s41378-022-00377-z, 20221 8.
[50] G. Zhang, J. Huang, L. Wang, Z. Geng, D. Zhang, J. Liu, G. Zhang, J. Huang, L. Wang, Z. Geng, D. Zhang, J. Liu, Design and preparation of anti-reflection nanoarray structure on the surface of space solar cell glass cover, Coatings 13 (2023) 1092, https://doi.org/10.3390/COATINGS13061092, 2023Page 1092 13.
[51] G. Jia, Z. Ji, H. Wang, R. Chen, Preparation and properties of five-layer graded-refractive-index antireflection coating nanostructured by solid and hollow silica particles, Thin. Solid. Films. 642 (2017) 174–181, https://doi.org/10.1016/J.TSF.2017.09.038.
[52] Q. Yu, S. Chan, K. Chen, B. Zhao, X. Ren, G. Pei, Numerical and experimental study of a novel vacuum photovoltaic/thermal (PV/T) collector for efficient solar energy harvesting, Appl. Therm. Eng. 236 (2024) 121580, https://doi.org/10.1016/J.APPLTHERMALENG.2023.121580.